


Spring 5-2012

# Large, Long-Lived Convective Systems Over Subtropical South America and Their Relationships With Atmospheric Teleconnections

Kyle Mattingly

Western Kentucky University, [kyle.mattingly842@topper.wku.edu](mailto:kyle.mattingly842@topper.wku.edu)

Follow this and additional works at: [http://digitalcommons.wku.edu/stu\\_hon\\_theses](http://digitalcommons.wku.edu/stu_hon_theses)

 Part of the [Atmospheric Sciences Commons](#), [Environmental Sciences Commons](#), and the [Meteorology Commons](#)

---

## Recommended Citation

Mattingly, Kyle, "Large, Long-Lived Convective Systems Over Subtropical South America and Their Relationships With Atmospheric Teleconnections" (2012). *Honors College Capstone Experience/Thesis Projects*. Paper 353.  
[http://digitalcommons.wku.edu/stu\\_hon\\_theses/353](http://digitalcommons.wku.edu/stu_hon_theses/353)

This Thesis is brought to you for free and open access by TopSCHOLAR®. It has been accepted for inclusion in Honors College Capstone Experience/Thesis Projects by an authorized administrator of TopSCHOLAR®. For more information, please contact [connie.foster@wku.edu](mailto:connie.foster@wku.edu).

LARGE, LONG-LIVED CONVECTIVE SYSTEMS OVER SUBTROPICAL SOUTH  
AMERICA AND THEIR RELATIONSHIPS WITH ATMOSPHERIC  
TELECONNECTIONS

A Capstone Experience/Thesis Project

Presented in Partial Fulfillment of the Requirements for

the Degree Bachelor of Science with

Honors College Graduate Distinction at Western Kentucky University

By

Kyle S. Mattingly

\* \* \* \* \*

Western Kentucky University  
2012

CE/T Committee:

Professor Joshua Durkee, Advisor

Professor Gregory Goodrich

Professor James Navalta

Approved by

\_\_\_\_\_  
Advisor

Department of Geography and Geology

Copyright by  
Kyle S. Mattingly  
2012

## ABSTRACT

This study provides a climatological assessment of persistent elongated convective systems (PECS) over subtropical South America during the austral warm seasons of 1998-2007 and a comparison of PECS frequency and physical characteristics to mesoscale convective complexes (MCCs) in the region. Relationships between the Antarctic Oscillation (AAO) and El Niño – Southern Oscillation (ENSO) teleconnections and large, long-lived convective systems (LLCSs) are explored. An average of 143 PECS and 37 MCCs occurred per warm season. PECS lasted longer on average than MCCs (17 hrs. vs. 14 hrs.) and reached a greater average maximum cloud-shield extent than MCCs (297,300 km<sup>2</sup> vs. 256,500 km<sup>2</sup>). PECS frequency was maximized over the La Plata river basin during December – February. The relative frequency of LLCS occurrence was greatest during negative AAO phases (0.906 LLCSs/day) and positive ENSO phases (28.1 LLCS/month). LLCS maximum cloud-shield extent was greatest during negative AAO phases and positive ENSO phases. LLCSs tended to be displaced southward during negative AAO phases and neutral ENSO phases. These results suggest that AAO and ENSO phases have at least some influence on LLCSs over SSA. Additionally, the high relative frequency of PECS compared to MCCs suggests they may contribute substantially to yearly precipitation totals in the region.

Keywords: Climatology, Meteorology, South America, Mesoscale Convective Systems, Atmospheric Teleconnections

## ACKNOWLEDGEMENTS

Throughout my time at WKU, I have been fortunate to receive inspiration and support from the outstanding faculty and students in both the Department of Geography and Geology and in the Honors College. I am grateful to Joshua Durkee, my CE/T advisor, for his invaluable expertise, encouragement, and enthusiasm throughout the CE/T process, and for the original inspiration for this research. Gregory Goodrich, my academic advisor and CE/T second reader, has been a constant source of wisdom and advice since I first stepped on campus. Other faculty members in the department, particularly Xingang Fan, Stuart Foster, and Rezaul Mahmood, have aided my academic and personal development by being great teachers and great people.

I would like to thank the Honors College for cultivating a challenging and stimulating academic environment. Honors classes and events have truly been a highlight of my time at WKU, and I have received excellent support from Honors faculty throughout the CE/T process. In particular, I am grateful to James Navalta for his participation as third reader and willingness to devote his time and energy to the development of young scholars.

## VITA

June 30, 1989	Born – Owensboro, KY
2008	Owensboro Catholic High School, Owensboro, KY
2008	National Merit Finalist
2009-2011	Quality Assurance Technician, Kentucky Mesonet
2010	National Oceanic and Atmospheric Administration Ernest F. Hollings Scholar
Summer 2011	Research project “Thermodynamic Characteristics of New England Tornadoes” completed during internship at National Weather Service Gray, ME

## FIELDS OF STUDY

Major Field: Meteorology

Minor Field: Mathematics

## TABLE OF CONTENTS

	<u>Page</u>
Abstract	ii
Acknowledgements	iv
Vita	v
List of Tables and Figures	viii
Chapters:	
1. Introduction	1
2. Background	3
a. Mesoscale Convective Complexes	3
b. Persistent Elongated Convective Systems	5
c. Atmospheric Teleconnections Affecting Subtropical South America	7
i. El Niño – Southern Oscillation	8
ii. Antarctic Oscillation	9
3. Data and Methodology	13
4. Results	15
a. PECS vs. MCCs	16
b. Temporal Characteristics of PECS	17
c. Spatial Characteristics of PECS	19
d. Atmospheric Variability and LLCs	20
i. Relationships Between the AAO and LLCs	21



	<u>Page</u>
ii. Relationships Between ENSO and LLCs	23
iii. Interactions Between the AAO, ENSO, and LLCs	25
5. Conclusions and Discussion	28
References	33
Appendix A: Tables	40
Appendix B: Figures	43

## LIST OF TABLES AND FIGURES

<u>Table</u>		<u>Page</u>
1	Mesoscale Convective Complex Definition	40
2	Frequency of LLCS occurrence over combinations of monthly ENSO and daily AAO phases	41
3	Independent-sample t-tests for difference of means between AAO phases under various ENSO background conditions	42
<u>Figure</u>		
1	Ocean-atmosphere features in the equatorial Pacific during different ENSO phases	43
2	Linear regression of ENSO index with global precipitation anomalies and correlations between the ENSO index and precipitation anomalies	44
3	Correlation maps between AAO index and bi-monthly precipitation anomalies over SSA	45
4	Sample scenes of GOES imagery used to compile LLCS dataset	46
5	Number of PECS and MCCs, average PECS and MCC duration, and average PECS and MCC maximum area for each warm season	47
6	Intraseasonal distribution of PECS and MCCs	48
7	Intraseasonal distribution of maximum $< -52$ °C cloud shield area attained by PECS and MCCs	49
8	Intraseasonal distribution of duration of PECS and MCCs	50

<u>Figure</u>	<u>Page</u>
9 Scatter plot of duration and maximum extent for all PECS and MCCs	51
10 Diurnal distribution of PECS and MCC critical stages	52
11 Intraseasonal distribution of eccentricity of < -52 °C cloud shields associated with PECS, MCCs, and all LLCs at time of maximum extent	53
12 Point density map of all PECS centroids	54
13 Point density map of location PECS centroids at time of initiation, maximum cloud-shield extent, and termination	55
14 Latitude of PECS and MCC centroids at critical stages	56
15 Intraseasonal distribution of latitude of PECS and MCC centroids at all points in their life cycles	57
16 Time series of daily AAO index for entire study period	58
17 Distribution of daily AAO index values for entire study period and on days when an LLCs occurred	59
18 Maximum extent reached by LLCs during various AAO phases	60
19 Latitude of LLCs centroids during various AAO phases	61
20 LLCs duration during various AAO phases	62
21 Eccentricity of LLCs cloud shields at time of maximum extent during various AAO phases	63
22 Correlation between number of LLCs during each month and the monthly ENSO index	64
23 Maximum extent reached by LLCs during various ENSO phases	65
24 Latitude of LLCs centroids during various ENSO phases	66
25 LLCs duration during various ENSO phases	67
26 Eccentricity of LLCs cloud shields at time of maximum extent during various ENSO phases	68

27	Time series of monthly AAO index and monthly ENSO index for entire study period	69
28	Relationship between the monthly ENSO index and the daily AAO index, and between the monthly AAO and ENSO indices for entire study period	70
29	Relationship between the daily AAO index and LLCS maximum cloud-shield extent during various ENSO phases	71
30	Relationship between the daily AAO index and latitude of LLCS centroids during various ENSO phases	72
31	Relationship between the daily AAO index and LLCS duration during various ENSO phases	73
32	Relationship between the daily AAO index and eccentricity of LLCS cloud shields during various ENSO phases	74

## CHAPTER 1

### INTRODUCTION

Many regions throughout the world are subject to the frequent occurrence of extensive thunderstorm complexes during the warm season. These mesoscale convective systems (MCSs), composed of individual thunderstorms that have organized into a contiguous precipitation shield, are notable for the large spatial and temporal dimensions that they sometimes attain. MCSs are capable of producing many types of hazardous weather, such as large hail, high winds, and tornadoes (Maddox 1980; Houze et al. 1990). They also are notable for the substantial amounts of precipitation they can produce (Tollerud and Collander 1993) and frequently lead to flooding and flash flooding issues (Rodgers et al., 1983; Anderson and Arritt, 1998).

Numerous studies have shown that MCSs play a prominent role in the long-term hydrologic budget of areas such as the central United States (Fritsch et al., 1986; Ashley et al., 2003), the Sahel region of Africa (Laing et al., 1999; Mathon et al., 2002), and subtropical South America (Mota, 2003; Viana, 2006; Salio and Nicolini, 2007; Durkee et al., 2009). Subtropical South America, the focus of this study, is home to the La Plata River basin, which contains 30% of the earth's fresh water supply and is the fifth largest river basin in the world (Durkee and Mote, 2009). The La Plata region is one of the

largest food producers in the world, with an economy that is largely based on agriculture. The majority of the region's electricity is generated by hydropower plants on its numerous rivers (the Itaipú hydroelectric plant on the Paraná River alone generates over 95% of Paraguay's electricity and 24% of Brazil's), and most drinking water in the region (including that of Buenos Aires and São Paulo, the two largest cities in South America) is supplied by these rivers (Mechoso et al., 2001). Thus it is clear that the La Plata region is highly vulnerable to fluctuations in rainfall, and any shortages or excesses in precipitation result in major economic and social impacts on the region.

In order to more fully understand the characteristics and variability of the mesoscale convective systems that play a critical role in the hydrological budget of subtropical South America, this study first presents a climatology of Persistent Elongated Convective Systems (PECS) to supplement previous studies of Mesoscale Convective Systems (MCCs) over the region. The frequency and characteristics of both PECS and MCCs are then examined for relationships with the Antarctic Oscillation (AAO) and El Niño – Southern Oscillation (ENSO) teleconnections in an effort to enhance the predictability of these systems under varying phases of these large-scale modes of variability.

## CHAPTER 2

### BACKGROUND

#### **a. Mesoscale Convective Complexes**

A large portion of prior research pertaining to mesoscale convective systems has focused on the subclass of MCSs known as the mesoscale convective complex (MCC). Based on characteristics derived from infrared satellite imagery, Maddox (1980) defined the parameters that the cloud shield associated with a convective system must meet in order to be classified as an MCC. Maddox's original definition stated that MCCs must have a contiguous mass of cloud-top temperatures  $\leq -32$  °C with an area of  $\geq 100,000$  km<sup>2</sup> and an interior contiguous mass of cloud tops with temperatures  $\leq -52$  °C and an area of  $\geq 50,000$  km<sup>2</sup>; however, subsequent studies (e.g., Augustine and Howard, 1988; Jirak et al., 2003; Durkee and Mote, 2009) dropped the outer  $\leq -32$  °C cloud shield requirement based on observations that most precipitation occurs underneath the inner  $\leq -52$  °C cloud shield and that  $\leq -32$  °C cloud shields often encompass several distinct storm systems. These updated criteria are outlined in Table 1 and are used to define MCCs and PECS in this study. The most important aspect that defines the MCC as a distinct class of MCSs is its quasi-circular shape; the eccentricity (minor axis / major axis) of its  $\leq -52$ °C cloud shield area must be at least 0.7 at the time when this cloud shield reaches its maximum

extent. MCCs must also sustain a  $\leq -52^{\circ}\text{C}$  cloud shield area of at least 50,000 km<sup>2</sup> for over six hours, although the cloud shield does not have to maintain an eccentricity of  $\geq 0.7$  for its entire life cycle.

Previous studies have determined the regions of the world where mesoscale convective system activity commonly occurs. These include North and South America (Maddox, 1980; Guedes, 1985; Velasco and Fritsch, 1987; McAnelly and Cotton, 1989, among others), Africa (Laing, 1992; Laing and Fritsch, 1993a; Laing et al., 1999), India (Laing, 1992; Laing and Fritsch, 1993b), China (Miller and Fritsch, 1991), Australia (James, 1992), and Europe (Laing and Fritsch, 1997). Laing and Fritsch (2000) studied the large-scale environments associated with MCSs in several of these locations (Africa, Australia, China, South America, and the United States) and found that in each region, MCSs typically form in baroclinic zones where local maxima of lower-tropospheric vertical wind shear and convective available potential energy (CAPE) are present. The impetus for initial storm development is provided by a low-level jet (LLJ) transporting high potential temperature ( $\theta_e$ ), low static stability air, which is then forced to ascend when it encounters the shallow surface-based layer of cool air in the baroclinic zone. Other features of MCS development environments include a local maximum in absolute humidity, a strongly veering wind profile in the near-surface layer, an approaching weak mid-level shortwave trough, and an upper-level jet near the area of initial development. In the subtropical South America (SSA) development region, the LLJ fosters the formation of MCSs by transporting high  $\theta_e$  air from the tropical Amazon River basin southward into the La Plata basin of southeastern South America (Laing and Fritsch, 2000; Vera et al., 2006; Salio et al., 2007). Durkee and Mote (2009) also suggest that the



Andes Mountains, much like the Rocky Mountain range of North America, play an important role in the preconditioning environment for MCSs by providing a source of cold air advection aloft that acts to steepen lapse rates and decrease stability.

Durkee and Mote (2009, hereafter DM09) examined a climatology of warm-season (October - May) MCC activity in subtropical South America for 1998-2007. They found that the region experienced an average of 37 MCCs per warm season, with peak diurnal activity occurring during the overnight hours and a spatial concentration between 30°S and 20°S during December and January. The authors also noted that MCCs over SSA occur more frequently than over North America and are both larger (average size of 256,500 km<sup>2</sup> vs. a maximum size of 164,600 km<sup>2</sup> for North American MCCs) and longer-lasting ( $\bar{x} = 14$  h vs.  $\bar{x} = 10$  h) on average than North American MCCs. In a related study, Durkee et al. (2009) examined the contributions that MCCs make to rainfall totals across the same region. They determined that MCCs account for a considerable portion of total warm season precipitation in SSA, with 11%-20% of the total rainfall in most warm seasons provided by MCCs in much of the study domain. On smaller temporal and spatial scales, MCCs often had a greater impact. For example, MCCs accounted for 30%-50% of December precipitation in northern Argentina and portions of Paraguay, while provinces in west-central Argentina received up to 66% of their November rainfall from MCCs.

#### **b. Persistent Elongated Convective Systems**

Another subclass of MCSs, persistent elongated convective systems (PECS, first defined by Anderson and Arritt, 1998), are very similar to MCCs but have been studied much less extensively. PECS meet all MCC criteria except the eccentricity requirement

(see Table 1); PECS have an eccentricity of 0.2 to 0.7 at the time of their maximum cloud-shield extent and therefore tend to be more elongated or linear in shape rather than quasi-circular at the point in time when they reach their peak size. This minimum eccentricity parameter of 0.2 was established to ensure that long lines of convection without an internal circulation were not classified as PECS. Together, MCCs and PECS form a class of MCSs known as large, long-lived convective systems (LLCSs) (Nieto Ferreira et al., 2003).

Currently, there are no studies that provide a climatological analysis of MCSs in SSA, beyond the MCC work by DMO9 and Durkee et al. (2009). However, the MCC definition limits our understanding of MCSs because of the specific criteria used to classify such events. Therefore, a climatological understanding of PECS with respect to the MCC research by DM09 is necessary in order to provide an accurate account of the characteristics of large, long-lived convective systems (LLCS) over SSA. Anderson and Arritt (1998) found PECS to be more numerous than MCCs over North America during the warm seasons of 1992-93, while Jirak et al. (2003) found that PECS in the United States were more frequent, larger, more commonly associated with severe weather reports, and produced greater average rainfall amounts than MCCs and other MCSs during the warm seasons of 1996-98. It is quite possible that the outcome is similar for subtropical South America. Since PECS are quite similar to MCCs in every respect except their shape, it is likely that they have similar, if not greater, hydrological impacts on the region as MCCs. The first part of this study will provide climatological descriptions for PECS over subtropical South America for the warm seasons of 1998-2007.

### **c. Atmospheric Teleconnections Affecting Subtropical South America**

The second phase of this study will consider the possible influence of atmospheric teleconnections on Mesoscale Convective System activity in the SSA study region. Defined by statistically significant simultaneous correlations between meteorological variables at widely separated points on earth (Wallace and Gutzler, 1981; Mo and White, 1985), teleconnections are identified whenever it is found that anomalies in the current state of the atmosphere in one region can explain a significant proportion of the variance in other meteorological variables at distant locations. The importance of teleconnections lies in the ability to explain and forecast the variability in atmospheric variables at time scales of weeks and months (Mo and White, 1985; Barnston and Livezey, 1987).

Several major teleconnections have been identified through various analysis techniques (Wallace and Gutzler, 1981) and are used frequently in climate analysis and forecasting applications. These include the El Niño - Southern Oscillation pattern (ENSO) first noted by Hildebrandsson (1897) and later detailed by Walker and Bliss (1932), the Arctic Oscillation (AO) or Northern Annular Mode (Lorenz, 1951; Thompson and Wallace, 1998) and the North Atlantic Oscillation (NAO) (Walker and Bliss, 1932; Wallace and Gutzler, 1981), the Pacific North American pattern (PNA) (Wallace and Gutzler, 1981; Barnston and Livezey, 1987), the Madden-Julian Oscillation (MJO) (Madden and Julian, 1971; Hendon and Salby, 1994), and the Antarctic Oscillation (AAO) or Southern Annular Mode (SAM) (Rogers and Van Loon, 1982; Gong and Wang, 1999; Thompson and Wallace, 2000), among others. Teleconnections which have been closely linked to atmospheric variability over subtropical South America are ENSO

and the Antarctic Oscillation / Southern Annular Mode (hereafter AAO), and it is on these two that this study will focus with respect to convective systems.

### **i. El Niño – Southern Oscillation**

ENSO, considered the most dominant global teleconnection pattern on time scales of a few months to a few years, consists of a “seesaw” in sea surface temperature (SST) and sea-level pressure in the tropical Pacific that occurs semi-regularly on time scales of 2-7 years (Walker and Bliss, 1932; Bjerknes, 1969; National Research Council, 1983, among others). The influence of this quasi-periodic oscillation is felt throughout the world, with well-documented changes in the atmospheric circulation extending to the mid- and high-latitudes, in addition to the tropics, during positive and negative ENSO phases (Horel and Wallace, 1981; Hoskins and Karoly, 1981; Trenberth et al., 1998, among others). Figure 1 shows that during positive or warm phases of ENSO, referred to as El Niño, SSTs in the central and eastern equatorial Pacific rise significantly above the climatological average and a corresponding positive anomaly in sea-level pressure is observed in the western Pacific. This leads to positive anomalies in convection across the central and eastern equatorial Pacific. The opposite occurs during negative phases (La Niña), when SSTs off the western coast of Peru and into the central Pacific drop below normal (Trenberth, 1997). These SST anomalies are typically most pronounced during the northern hemisphere cool season (i.e., October through March), when their modifications of convective patterns in the tropics alter the

generation and propagation of atmospheric Rossby waves throughout the subtropics and mid-latitudes (Hoskins and Karoly, 1981; Held et al., 1989).

Warm-season precipitation anomalies in portions of southeastern South America, the region this study focuses on, have been shown by numerous studies to be related to ENSO phases (Ropelewski and Halpert, 1987, 1989, and 1996; Lau and Sheu, 1988; Rao and Hada, 1990; Pisciottano et al., 1994; Grimm et al., 2000; Barros and Silvestri, 2002). Specifically, these studies have shown that precipitation in Uruguay, southeastern Brazil, southern Paraguay, and northern Argentina tends to be above the median from around November to February (austral spring and summer) during El Niño events (see figure 2), with the opposite effect occurring when La Niña conditions are present. These rainfall anomalies are tied to atmospheric circulation anomalies produced by ENSO phase shifts, with an enhancement in the upper-air circulation and cyclonic vorticity advection observed over SSA during the austral warm season under El Niño. The inverse is typically observed during La Niña events. Since mesoscale convective systems account for a sizable proportion of warm season rainfall across SSA (Durkee et al., 2009) and their development is influenced by the overall atmospheric circulation in the region, it is hypothesized that the frequency and characteristics of these systems may be modified by ENSO phases.

## **ii. Antarctic Oscillation**

The Antarctic Oscillation (AAO) is a zonally-symmetric mode of variability, which describes the large-scale alternation of atmospheric mass

between the middle and high latitudes of the Southern Hemisphere (Rogers and van Loon, 1982; Gong and Wang, 1999; Thompson and Wallace, 2000, among others). Like the Arctic Oscillation in the Northern Hemisphere, the AAO is a higher frequency oscillation than ENSO, with phase shifts that typically take place on time scales of weeks to months. The AAO exists year-round, but its influences are typically most pronounced during the late spring in the Southern Hemisphere (Thompson and Wallace, 2000). Positive phases of the AAO are associated with negative height anomalies over Antarctica and positive height anomalies over the mid-latitude regions of the Southern Hemisphere, and vice versa during negative AAO phases (Thompson and Wallace, 2000; Fyfe, 2003; Reboita et al., 2009). During negative AAO phases, the Southern Hemisphere storm track tends to be displaced toward lower latitudes, causing a greater frequency of extratropical cyclones in lower-latitude regions; this process is reversed during positive phases (Carvalho et al., 2005; Reboita et al., 2009). Examples of regional impacts of the AAO on locations throughout the Southern Hemisphere include anomalously cool and wet conditions over most of Australia during the positive phase of the AAO (Gillett et al., 2006; Hendon et al., 2006; Gupta and England, 2006) and wetter than average winters in South Africa when negative AAO conditions prevail (Reason and Rouault, 2005).

Several recent studies have investigated the impact of positive and negative AAO phases on precipitation in subtropical South America. Silvestri and Vera (2003) found that negative (positive) phases of the AAO are associated with increased (decreased) moisture convergence and precipitation over Paraguay,

southeastern Brazil, and northeastern Argentina during the months of November and December (see figure 3d). Gillett et al. (2006) also investigated relationships between the AAO and precipitation patterns across the region, but did not identify significant relationships between the two to confirm the work of Silvestri and Vera (2003). Reboita et al. (2009) found pronounced positive precipitation anomalies associated with the negative phase of the AAO in northern Argentina and southeastern Brazil during austral summer and fall, with less clear-cut results during spring. They showed that the positive phase of the AAO is correlated with negative precipitation anomalies over northern Argentina during summer and in southern Brazil during the fall, but differences in the placement of these positive and negative anomalies across the seasons lead the authors to conclude that the precipitation anomalies are not exactly symmetric between the AAO phases. Since the AAO has been shown to modify atmospheric circulation and precipitation patterns in SSA, particularly during the warm season, it is hypothesized that the characteristics and frequency of MCSs are influenced by the phase of the AAO.

In summary, the work of DM09 provided a climatological description of MCCs in SSA, but a similar study of PECS is needed to gain a more comprehensive understanding of LLCS activity in the region. Based on previous studies of PECS and MCCs in North America, it is hypothesized that PECS in SSA occur more frequently and tend to be larger and longer-lasting than MCCs. Moreover, the AAO and ENSO teleconnections have been shown to modify warm-season precipitation and atmospheric circulation patterns in SSA, and it is

hypothesized that they will influence the frequency and characteristics of LLCs in some manner. Therefore, the purposes of this study are to (1) describe the characteristics of warm-season PECS over SSA and compare them to MCCs for the same region, as well as over North America, and (2) to investigate the possible influences of ENSO and the AAO on the frequency and characteristics of LLCs over SSA.



## CHAPTER 3

### DATA AND METHODOLOGY

This study uses a dataset of all large, long-lived convective systems (LLCSs) observed during the warm seasons (October - May) of 1998-2007 over subtropical South America compiled by DM09. The systems were identified and tracked using 4-km three-hourly GOES-8 and GOES-14 infrared satellite imagery (figure 4) and a hybrid automated/manual cloud-top identification procedure. GOES satellite imagery was generally available at 3-hour time increments. The first step in the tracking procedure was to identify all cloud shields that met the “size” requirement outlined in table 1 using an automated cloud-top identification procedure similar to Augustine (1985). Empirical orthogonal function (EOF) analysis of pixel coordinates was then used to determine the eccentricity and orientation of cloud shields. The authors manually observed each sequence of satellite images to track splitting and merging cloud shields, similar to the approach of Machado et al. (1998). Each distinct system that maintained a  $< -52$  °C cloud shield area for over six hours (usually two consecutive image times) was classified as either a persistent elongated convective system or a mesoscale convective system, depending on its eccentricity at its maximum cloud-shield extent ( $> 0.7$  for MCCs,

between 0.2 and 0.7 for PECS). A more thorough description of this identification and tracking process can be found in DM09.

Attributes tracked at each time step include  $< -52$  °C cloud-shield areas, the latitude and longitude coordinates of cloud-shield centroids, and their eccentricities. These attributes were then used to define additional characteristics of each system, such as its duration, maximum cloud-shield extent, and its location, eccentricity, and size throughout its life cycle.

The first part of this study describes the characteristics of PECS, as the properties of MCCs in the same dataset have already been thoroughly described by DM09. The second part, regarding the influence of ENSO and the AAO on SSA convective activity, encompasses both PECS and MCCs (together called LLCs) in order to provide a more complete picture of the influence of teleconnections on convective activity in the region.

In order to determine the influence of ENSO and the AAO on LLCs over SSA, archived indices of the phase of each teleconnection were obtained for the study period from the National Oceanic and Atmospheric Administration's Climate Prediction Center (CPC). The CPC uses the monthly Oceanic Niño Index (ONI), which is based on a 3-month running mean of SST anomalies from the 1971-2000 mean in the tropical Pacific, to evaluate the phase of ENSO during each month. Months where the ONI exceeds  $\pm 0.5$  are classified as warm (El Niño) or cool (La Niña) episodes, respectively. To evaluate the AAO, the CPC uses the daily AAO index, which is calculated by projecting the daily 700 hPa height anomalies onto the leading mode of Empirical Orthogonal Function (EOF) analysis of monthly mean 700 hPa height during the 1979-2000 period, then standardizing this value by the standard deviation of the monthly AAO index from 1979-

2000. Monthly data is used to characterize the ENSO phase because of the low-frequency nature of the oscillation, while the daily AAO index is used in the analysis because it was observed to change phase regularly on sub-monthly time scales.

## CHAPTER 4

### RESULTS

#### **a. PECS vs. MCCs**

Compared to the results of DM09, PECS over subtropical South America were considerably more frequent, larger, and longer-lasting than MCCs for the warm seasons of 1998-2007. Specifically, 1286 PECS and 330 MCCs occurred during the study period, with the mean ratio of PECS to MCCs 4:1 for each season (figure 5a). On average, 143 PECS and 37 MCCs occurred per warm season; this difference in means is significant at the 99% confidence interval ( $p = 0$ ). PECS lasted on average 17 hours, compared to 14 hours for MCCs ( $p = 0$ ), and lasted longer on average than MCCs during each season (figure 5b). PECS maximum cloud shield areas were nearly 41,000 km<sup>2</sup> larger on average than those of MCCs (297,300 km<sup>2</sup> vs. 256,500 km<sup>2</sup>,  $p = 0.001$ ), and PECS were larger on average than MCCs in every season except 2005-06 (figure 5c).

The higher frequency of PECS relative to MCCs over SSA is in agreement with the relationship in the United States detailed by Anderson and Arritt (1998), who found that PECS outnumbered MCCs 121 to 55 in the United States during 1992 and 1993 (average PECS to MCCs ratio of 2.2:1 for each season). Like this study, their results show that PECS reached larger maximum cloud shield sizes than MCCs on average in the

U.S.; in 1992, the average MCC maximum cloud-shield area was 145,100 km<sup>2</sup> and the average PECS maximum cloud-shield area was 188,000 km<sup>2</sup>, while in 1993 these values were 184,300 km<sup>2</sup> and 193,200 km<sup>2</sup>, respectively. However, they did not find a tendency for U.S. PECS to persist longer than MCCs; average duration was 10 hrs. for MCCs and 12 hrs. for PECS in 1992, but in 1993, average MCC duration was 14 hrs. compared to 12 hrs. for PECS.

#### **b. Temporal Characteristics of PECS**

In general agreement with the monthly distribution of MCCs described by DM09, the peak of PECS activity occurred during December - March (figure 6). However, there are some discrepancies in the distribution of PECS and MCCs. PECS frequency exhibited a definitive peak in January with February and March slightly more frequent than December. Meanwhile, MCC frequency exhibited a broader peak in December and January, while MCC frequency during February and March was less. Frequency differences also occurred near the beginning of the austral warm season, as PECS were more numerous in October than November, while the opposite was true for MCCs.

The median maximum cloud-shield area obtained by PECS was greatest during October, with a gradual decrease throughout the warm season until a minimum in March and April and a notable increase during May (figure 7a). This is in broad agreement with the MCC results of DM09, although there are once again a few notable dissimilarities. First, MCC maximum cloud-shield areas were at a minimum during February with a steady increase throughout the rest of the warm season; MCCs also showed a tendency to be smaller in October than in November.

The intraseasonal distribution of the duration of PECS was similar to the trend in maximum cloud-shield areas in that it resembled a quadratic curve with maxima during the transition seasons. However, unlike the trend in maximum cloud-shield area, the curve was nearly symmetrical around a minimum in PECS duration in January and the median duration of May PECS was higher than the median in October and November (figure 8a). This intraseasonal duration trend matches well with the monthly MCC duration characteristics found by DM09, with the only notable exception during May, where DM09 found a slight decrease in MCC durations compared to April. Moreover, a moderate correlation of 0.537 was found between PECS lifecycle duration and maximum cloud-shield area (figure 9a), which corresponds well with the value of 0.560 for MCCs calculated by DM09.

The diurnal distribution of PECS critical stages (figure 10), in agreement with the MCC results of DM09, displays a tendency for PECS activity to be maximized during the late afternoon through early morning hours. PECS initiation was most frequent at the times of 1745 UTC and 2045 UTC, or in the mid to late afternoon hours (local time is either 3 or 4 hours behind UTC). The majority of PECS then reached their maximum cloud-shield extent during the evening hours of 2045 through 0245 UTC. Interestingly, the distribution of termination times did not contain the defined peaks observed in initiation and maximum cloud-shield extent, but instead was distributed more evenly throughout the day, with a relatively minor peak occurring from 2345 UTC through 0245 UTC. The observed tendency for PECS over SSA to be primarily nocturnal is in general agreement with previous studies of MCCs and PECS in other regions such as the U.S. (Anderson and Arritt, 1998), Africa (Laing and Fritsch, 1993a), and India (Laing and

Fritsch, 1993b). However, the findings presented in this study show a tendency for LLCs over SSA to initiate and reach their maximum cloud-shield extent several hours earlier than in these other regions.

Lastly, the intraseasonal variability in the eccentricity of the  $< -52$  °C cloud shields of PECS, MCCs, and all LLCs during their maximum extent was examined (figure 11). No discernible trend in cloud-shield eccentricity was observed for the majority of the warm season, except for a pronounced decrease in May relative to the preceding months. However, it is important to note that the median eccentricity of all LLC cloud shields is 0.48, with a median of 0.45 for PECS and 0.79 for MCCs. This demonstrates the increased frequency of PECS compared to MCCs and emphasizes the value of relaxing the MCC eccentricity requirement in order to gain a more complete understanding of Mesoscale Convective System activity in the region.

### **c. Spatial Characteristics of PECS**

Figure 12 shows the highest concentration of PECS frequency during the nine warm seasons occurred over southern Paraguay, northeastern Argentina, northern Uruguay, and adjacent areas of southern and southeastern Brazil. Analysis of the location of PECS centroids during critical stages (figure 13) revealed that initiation most frequently occurred in the lee of the Andes over southern Bolivia and central Argentina, with another broader initiation maximum region across southern Brazil, southward through eastern Paraguay and into northern Argentina. During the time of maximum cloud-shield extent, PECS were most frequent over southern Brazil and eastern Paraguay and, to a lesser degree, central Argentina. Once PECS reached termination, the greatest

cloud-shield centroid density was located over southern Brazil. Taken in sequence, these maps suggest a tendency for PECS to form in the lee of the Andes, then propagate eastward due to the influence of upper tropospheric westerlies. A box plot of the latitudinal variation of PECS centroids during each critical stage (figure 14a) also reveals a slight equatorward progression in their location throughout their life cycle similar to the MCC results of DM09, with a majority of PECS concentrated between 20°S - 30°S.

The intraseasonal distribution of the latitude of all PECS centroids shows a clear warm-season pattern in PECS location (figure 15a). The median location of PECS centroids was 28°S during October, with a slow equatorward progression until January. From January until May, the median latitude steadily migrated poleward, with a median latitude of around 33°S in May. As expected, this pattern is similar to the intraseasonal MCC migration pattern discovered by DM09, but with a few noteworthy discrepancies. First, DM09 found that MCCs have a lower median latitude (closer to the equator) in November and February than in December and January, which contrasts with the smooth high-low-high intraseasonal latitude trend found in this study for PECS. Second, for all months except December and January, the median latitude of PECS centroids was poleward of the MCC median latitude determined by DM09.

#### **d. Atmospheric Variability and LLCs**

In order to examine relationships between the Antarctic Oscillation, ENSO, and large, long-lived convective system (LLCS) activity over SSA, the MCC dataset of DM09 was merged with the PECS dataset used in the preceding sections of this study. The resulting sum of every  $< -52$  °C cloud shield with an area greater than 50,000 km<sup>2</sup>



and an eccentricity of  $\geq 0.2$  that persisted for at least 6 hours during the warm seasons of 1998 – 2007 was 1616 LLCs. Each day in the 1998-2007 study period was classified according to the phase of the AAO and ENSO indices following the criteria outlined in the sections below. Comparisons of relative LLC frequency between phases were made by dividing the number of LLCs that reached their maximum cloud-shield extent on days when the given phase was in place by the total number of days the teleconnection was in the given phase.

#### **i. Relationships Between the AAO and LLCs**

In order to determine the influence of the AAO on LLC activity, each LLC was classified by the daily AAO index for the day on which the given LLC reached its maximum cloud-shield extent. Negative phases of the AAO were defined as days when the AAO index was less than -1.5, neutral phases had an AAO index of greater than or equal to -1.5 and less than or equal to 1.5, and positive phases were classified as days when the AAO index was greater than 1.5. These boundaries were chosen based on the observation that the standard deviation of the daily AAO index for all days in the study period was 1.33. Figure 16 shows that the daily AAO index is subject to large variations and swings between positive, neutral, and negative phases on daily to weekly time scales, and it is for this reason that the daily index was used in the analysis rather than a monthly composite.

Overall, 2188 days were included in the 1998-2007 study period. The AAO index was considered positive for 319 (14.6%) of these days, neutral for

1581 days (72.2%), and negative for the remaining 288 days (13.2%). Out of the 1616 LLCs recorded, 261 occurred on the negative AAO days (0.906 LLCs/day), 1157 (0.732 LLCs/day) occurred during an AAO phase classified as neutral, and the other 198 (0.621 LLCs/day) occurred on days when the AAO was in a positive phase. This increased rate of LLC activity during strongly negative AAO phases is reflected in figure 17, which shows that the AAO index is skewed towards the positive end for all days in the period of record (figure 17a), but tends to be more negative on days when LLCs occur (figure 17b).

Four characteristics of LLCs were examined for possible relationships with the AAO: maximum cloud-shield extent, latitude of system center and eccentricity during maximum extent, and duration. Figure 18 shows that the maximum cloud-shield extent of LLCs showed a decreasing trend from negative to positive AAO phases. Independent sample difference of means t-test results showed that the difference in means of maximum cloud-shield extent between negative and positive AAO phases and between neutral and positive AAO phases was statistically significant at the 95% confidence level (p-values of 0.01 and 0.04, respectively). Meanwhile, the difference in means between negative and neutral AAO phases was not significant. The median latitude of LLC centroids during maximum extent increased from negative to positive phases (figure 19). T-tests showed that the difference in means between the negative phase and the neutral phase and between the negative phase and the positive phase were both statistically significant at the 99% confidence level ( $p = 0.01$  in both cases). The median duration of LLCs (figure 20) was smaller during positive phases than

during neutral or negative phases of the AAO. However, t tests showed that the differences in means between the three categories were not statistically significant ( $p = 0.48, 0.72, \text{ and } 0.89$ , respectively). Finally, there was no statistical difference in mean eccentricities across varying AAO phases (figure 21).

## **ii. Relationships between ENSO and LLCs**

In order to examine the relationship between ENSO and LLC activity, archived monthly ENSO index data was obtained from the Climate Prediction Center. Monthly data was chosen because the ENSO cycle is not subject to daily and weekly fluctuations like the AAO, but instead varies on monthly to seasonal time scales (see figure 27). Definitions of the negative, neutral, and positive phases of ENSO were based on the Climate Prediction Center's criteria: an index of less than  $-0.5$  denotes a negative (La Niña) phase,  $-0.5$  to  $0.5$  is neutral, and greater than  $0.5$  is positive (El Niño). Months when the index was exactly  $-0.5$  or exactly  $0.5$  were included in the neutral category.

Out of the 72 months in the study period, 22 (30.6%) were associated with negative ENSO, 35 (48.6%) with neutral ENSO, and the remaining 15 (20.8%) with positive ENSO conditions. Out of the 1616 LLCs, 499 occurred during negative ENSO phases (22.7 LLCs/month), 695 occurred during neutral ENSO conditions (19.9 LLCs/month), and the remaining 422 occurred during positive ENSO months (28.1 LLCs/month). As figure 22 shows, a very weak positive correlation (0.07) was determined for the monthly ENSO index and the number of LLCs that occurred in each month.

As with the AAO index, the LLCS characteristics of maximum cloud-shield extent, latitude and eccentricity during time of maximum extent, and duration were examined for relationships with the ENSO index. Independent sample t-tests were used to determine statistical significance in the difference in means between ENSO phases. Figure 23 shows that the median maximum cloud-shield extent of LLCS cloud shields increased from negative to positive ENSO phases. The difference in means between negative and positive ENSO phases, and between neutral and positive phases was determined to be statistically significant at the 95% level (p-values of 0.002 and 0.03, respectively). The latitude of LLCS centroids during maximum extent (figure 24) exhibits a tendency for LLCSs to be located at lower latitudes during both negative and positive ENSO phases, which a poleward location during neutral ENSO conditions. These differences in means were statistically significant ( $> 95\%$  confidence interval) for all three phase comparisons (negative vs. neutral, negative vs. positive, neutral vs. positive), with p-values of 0, 0.02, and 0.004. LLCSs showed a statistically significant tendency ( $> 95\%$  confidence interval) to last for shorter durations during negative ENSO conditions vs. neutral and positive conditions (figure 25), with p-values of 0.003 for the negative vs. neutral case, and 0.05 for the negative vs. positive case. LLCS eccentricity during maximum extent (figure 26) did not, however, demonstrate any statistically significant relationships between all ENSO phases.

### **iii. Interactions between the AAO, ENSO, and LLCSs**

The last piece of this study focused on possible relationships between the AAO and ENSO and the combined impacts of these teleconnections on LLCS activity. Figure 27 suggests a possible inverse relationship between the two, as fluctuations in the monthly ENSO index were often matched with shifts in the opposite direction of the monthly AAO index, especially during the early seasons of the study period. This connection is somewhat supported by figure 28, which shows a -0.36 correlation coefficient between the monthly ENSO index and the monthly AAO index (figure 28b) and a -0.26 correlation coefficient (figure 28a) when the daily AAO index is considered. The goal of this section was to find which combinations of AAO and ENSO phases were associated with the highest frequency of LLCS events and to see how changes in ENSO phase, which take place on greater temporal and spatial scales than AAO variations, alter the smaller-scale relationships between the AAO and LLCS characteristics. To that end, the daily AAO index rather than the monthly version was used in this analysis.

Table 2 demonstrates how the frequency of LLCS occurrence varied between different paired phases of the AAO and ENSO. The first two rows of this table contain the raw frequency of number of LLCSs and total amounts of days in the period of record for the various pairings of AAO and ENSO phases, with the third row containing a relative frequency of LLCS occurrence for each phase pairing. These findings show that positive ENSO phases were associated with higher relative LLCS frequency than negative and neutral phases, regardless of

the AAO phase. The greatest relative frequency of LLCs occurs when a positive ENSO phase is paired with a neutral AAO phase (1.04 LLCs/day), followed closely by negative (0.99 LLCs/day) and positive (0.96 LLCs/day) AAO phases. During neutral and negative ENSO conditions, the negative phase of the AAO (0.87 and 0.85 LLCs/day) was associated with greater LLC frequency than positive (0.61 and 0.57 LLCs/day) and neutral phases (0.57 and 0.79 LLCs/day). The minimum average amount of LLC activity occurred when neutral ENSO and AAO phases were paired (0.57 LLCs/day), and when negative ENSO and positive AAO phases occurred simultaneously (0.57 LLCs/day).

Relationships between the AAO and characteristics of LLCs were investigated for possible changes correlated with the influence of negative, neutral, and positive ENSO background conditions. Figure 29 shows that during negative ENSO phases (figure 29a), the median maximum cloud-shield extent of LLCs decreased from negative to positive AAO phases, while there was less of a discernible AAO-related trend during neutral (figure 29b) and positive (figure 29c) background ENSO phases. The median latitude of LLC centroids during maximum extent (figure 30) increased from negative to positive AAO phases during neutral (figure 30b) and positive (figure 30c) ENSO phases. However, no AAO-related trend was apparent while the ENSO index was negative (figure 30a). Relationships between the AAO and LLC duration (figure 31) and eccentricity (figure 32) were more variable across ENSO phases, with few consistent trends emerging.

The statistical significance in the differences in means of each variable between each AAO category displayed in these plots is summarized in table 3. The lack of statistically significant differences in means of LLCS characteristics between AAO categories under various ENSO background conditions demonstrated in this table can be at least partially attributed to the dearth of observations in each category. Since the full dataset of LLCSs was divided first by ENSO category and then by AAO category, there were much fewer degrees of freedom than in the t-tests of previous sections, making statistical significance more difficult to determine.

## CHAPTER 5

### CONCLUSIONS AND DISCUSSION

This study provides a climatological assessment of warm-season persistent elongated convective systems (PECS) over subtropical South America for 1998-2007, and presents a comparative analysis between MCCs and PECS in the region. This type of analysis is needed to gain a more thorough understanding of mesoscale convective system activity in SSA, as previous studies were limited to only studying MCCs with a cloud-shield eccentricity of  $> 0.7$  during time of maximum cloud-shield extent. Relationships between the Antarctic Oscillation (AAO) and El Niño / Southern Oscillation (ENSO) teleconnections and the characteristics of large, long-lived convective systems (LLCSs) in the region are also delineated.

Overall, PECS were more frequent, larger, and longer-lasting than MCCs over SSA during the study period. An average of 143 PECS and 37 MCCs occurred during each warm season; this difference in means is significant at the 99% confidence interval ( $p = 0$ ). The average maximum cloud-shield extent of PECS was greater than the average found by Durkee and Mote (2009) for MCCs over SSA ( $297,300 \text{ km}^2$  vs.  $256,500 \text{ km}^2$ ,  $p = 0.001$ ), and PECS had a greater average duration than MCCs (17 hours vs. 14 hours,  $p = 0$ ). The median cloud-shield eccentricity at maximum cloud-shield extent for all PECS



and MCC events was 0.49, demonstrating that the distribution of LLCs is weighted toward PECS. PECS frequency peaked during the height of austral summer from December - February, with these months also marking a minimum in the average maximum cloud-shield extent and life-cycle duration. Similar to MCCs, PECS occurred most frequently during the late afternoon through late evening hours.

The highest concentration of PECS cloud-shield centroids was located in the region of southern Paraguay, northeastern Argentina, northern Uruguay, and adjacent areas of far southern Brazil. On average PECS initiate in the lee of the Andes and migrate toward the east-northeast before reaching maximum cloud-shield extent and later dissipating. From October through the peak of the warm season in January, PECS showed a steady seasonal equatorward migration, with a more pronounced poleward trend from January - May.

Both PECS and MCCs were included in the analysis of teleconnection influences on convective activity; together these two classes of systems are referred to as large, long-lived convective systems (LLCSs). Archived data for the daily Antarctic Oscillation index, obtained from the Climate Prediction Center, was used to associate LLCS frequency and other physical characteristics with negative (AAO index  $< -1.5$ ), neutral ( $-1.5 \leq \text{AAO index} \leq 1.5$ ) and positive (AAO  $> 1.5$ ) AAO phases. The average frequency of LLCS occurrence was greater during negative AAO phases (0.906 LLCSs/day) than during neutral (0.732 LLCSs/day) and positive (0.621 LLCSs/day) phases. The median maximum cloud-shield extent of LLCS cloud shields was greater during negative phases and less during positive phases, while the median latitude of LLCS centroids during maximum cloud-shield extent increased from negative to positive phases.

Monthly ENSO index data from the CPC was used to classify LLCS events according to negative (ENSO index  $< -0.5$ ), neutral ( $-0.5 \leq$  ENSO index  $\leq 0.5$ ), and positive (ENSO index  $> 0.5$ ) ENSO phases. LLCSs were most frequent during positive ENSO phases (28.1 LLCSs/month), with decreased frequency during negative (22.7 LLCSs/month) and neutral (19.9 LLCSs/month) phases. An increase in the maximum cloud-shield extent of LLCSs from negative to positive ENSO phases was observed, as was a tendency for LLCS centroids to be located at lower latitudes during positive and negative ENSO phases. Average LLCS duration was less during negative ENSO phases. Investigations of the relationships between the AAO, ENSO, and LLCS activity showed a weak to moderate negative correlation between the AAO and ENSO. The highest relative frequency of LLCS occurrence was associated with positive ENSO phases paired with neutral AAO phases. High LLCS relative frequency was also observed when a positive ENSO phase coincided with negative or positive AAO phases, and when a negative AAO phase occurred alongside neutral or negative ENSO phases. Statistical significance of variations in mean LLCS characteristics between AAO phases under varied ENSO background phases was difficult to establish due to a lack of observations.

Due to the limited temporal extent of this dataset, it is difficult to draw definitive conclusions about the effects of ENSO and the AAO on LLCSs over SSA. A full ENSO phase cycle often takes five years or more to complete, meaning that an LLCS dataset spanning at least 30 years is needed to establish unequivocal relationships between the two. Because the AAO typically oscillates on sub-monthly time scales, there is more confidence in the relationships detailed between the AAO and LLCSs in this study, but a larger dataset would also be desirable in this case. Despite these caveats, this study does

suggest that AAO and ENSO phases have at least some influence on LLCs in the region. The increased frequency and size of LLCs on days when the AAO index was less than -1.5 may possibly be connected to the equatorward displacement of the Southern Hemisphere storm track during negative AAO phases (Carvalho et al., 2005; Reboita et al., 2009). Further, the findings in this study that show increased LLC frequency during positive ENSO phases agrees with previous studies that have detailed an enhancement in the upper-level circulation, and an associated positive anomaly in precipitation over SSA during El Niño.

However, the decrease in LLC occurrence and maximum cloud-shield extent during neutral and positive AAO phases and during neutral and negative ENSO phases is not dramatic, which implies that the presence of strong westerlies or an extratropical cyclone is not an essential prerequisite to LLC formation in the region. In fact, LLCs tended to be located in closer proximity to the equator during positive AAO phases and negative ENSO phases, which suggests that mechanisms other than the direct influence of the synoptic-scale storm track are of greatest influence in the formation of LLCs. One possible explanation is that an increased meridional component to the upper-level flow and an associated increase in vorticity advection over the region during negative AAO phases and positive ENSO phases induces a stronger flow of warm, moist air from the tropics to the subtropics via an enhanced low-level jet. It bears mentioning that a trend toward the positive phase of the AAO has been noted in recent decades (Thompson and Wallace, 2000; Visbeck, 2009), and the results of this study suggests that this trend could have important implications for both LLC frequency and long-term precipitation totals in the region.

Lastly, the finding that PECS occur much more frequently than MCCs over SSA, as well as their apparent tendency to be larger and longer-lasting than MCCs, suggests that they play a prominent role in the annual hydrologic budget of the region. Durkee et al. (2009) showed that MCCs produce a substantial portion of yearly precipitation totals in SSA. For example, MCCs account for 11-20% of total annual rainfall during most warm seasons in much of SSA, with monthly contributions in portions of Argentina and Paraguay as much as 50-66%. Therefore, it is plausible to consider PECS-related rainfall would likely contribute to precipitation totals in a similar fashion. Given that climate model simulations predict an increase in the probability of future extreme precipitation events due to climate change (Wehner, 2004; Kharin and Zwiers, 2005; Kharin et al., 2007, among others), an assessment of the hydrologic impact of these large, long-lived convective systems that are capable of producing extreme amounts of precipitation is needed to form a baseline for comparison with future observations and model simulations. Other future studies should investigate the internal dynamics of PECS compared to MCCs. Given that PECS have been shown to be significantly larger and longer-lasting than MCCs, why don't they organize into quasi-circular forms like MCCs due to Coriolis influences? Can PECS generate inertially stable mesoscale convective vortices (MCVs) as MCCs sometimes do, and if so are they as frequent or as persistent as those associated with MCCs? Finally, future studies could investigate the relationships between LLCS activity in SSA and other teleconnections not considered in this study, particularly the Madden-Julian Oscillation.

## REFERENCES

- Ambrizzi, T., 2006: Chapter 3, Interannual low-frequency variability: background, in *Climate Change in La Plata Basin*. V. R. Barros, R. Clarke, and P. Silva Dias, Eds. CIMA - CONICET/UBA, ISBN 950-692-066-4, 35-43.
- Anderson, C. J. and R. W. Arritt, 1998: Mesoscale convective complexes and persistent elongated convective systems over the United States during 1992 and 1993. *Mon. Wea. Rev.*, **126**, 578–599.
- Ashley, W. S., T. L. Mote, P. G. Dixon, S. L. Trotter, E. J. Powell, J. D. Durkee, A. J. Grundstein, 2003: Distribution of mesoscale convective complex rainfall in the United States. *Mon. Wea. Rev.*, **131**, 3003–3017.
- Augustine, J. A., 1985: *An automated method for the documentation of cloud-top characteristics of mesoscale convective systems*. NOAA Tech. Memo. ERL ESG-10, NOAA/FSL, Boulder, CO, 121 pp.
- Augustine, J. A., and K. W. Howard, 1988: Mesoscale convective complexes over the United States during 1985. *Mon. Wea. Rev.*, **116**, 685–701.
- Barnston, A. G., and R. E. Livezey, 1987: Classification, seasonality and persistence of low-frequency atmospheric circulation patterns. *Mon. Wea. Rev.*, **115**, 1083–1126.
- Barros, V. R., G. E. Silvestri, 2002: The relation between sea surface temperature at the subtropical south-central Pacific and precipitation in southeastern South America. *J. Climate*, **15**, 251–267.
- Bjerknes, J., 1969: Atmospheric teleconnections from the equatorial Pacific. *Mon. Wea. Rev.*, **97**, 163–172.
- Carvalho, L. M. V., C. Jones, T. Ambrizzi, 2005: Opposite phases of the Antarctic Oscillation and relationships with intraseasonal to interannual activity in the

Tropics during the austral summer. *J. Climate*, **18**, 702–718.

Climate Prediction Center, cited 2012: Global ENSO temperature and precipitation linear regressions. [Available online at <http://www.cpc.ncep.noaa.gov/products/precip/CWlink/ENSO/regressions/geplr.shtml>.]

Durkee, J. D., and T. L. Mote, 2009: A Climatology of warm-season mesoscale convective complexes in subtropical South America. *Int. J. Climatol.*, doi:10.1002/joc.1961, in press.

Durkee, J. D., T. L. Mote, J. M. Shepherd, 2009: The contribution of mesoscale convective complexes to rainfall across subtropical South America. *J. Climate*, **22**, 4590–4605.

Fritsch, J. M., R. J. Kane, C. R. Chelius, 1986: The contribution of mesoscale convective weather systems to the warm-season precipitation in the United States. *J. Climate Appl. Meteor.*, **25**, 1333–1345.

Fyfe, J. C., 2003: Separating extratropical zonal wind variability and mean change. *J. Climate*, **16**, 863–874.

Gillett, N. P., T. D. Kell, P. D. Jones, 2006: Regional climate impacts of the Southern Annular Mode. *Geophys. Res. Lett.*, **33**, L23704, 4 pp.

Gong, D., and S. Wang, 1999: Definition of Antarctic Oscillation Index. *Geophys. Res. Lett.*, **26**, 459–462.

Grimm, A. M., V. R. Barros, M. E. Doyle, 2000: Climate variability in southern South America associated with El Niño and La Niña Events. *J. Climate*, **13**, 35–58.

Guedes, R. L., 1985: Condições de grande escala associadas a sistemas convectivos de mesoescala sobre a região central da América do Sul. Dissertação de Mestrado. IAG/USP, São Paulo, SP, 89 pp.

Sen Gupta, A., and M. H. England, 2006: Coupled ocean–atmosphere–ice response to variations in the Southern Annular Mode. *J. Climate*, **19**, 4457–4486.

Held, I. M., S. W. Lyons, S. Nigam, 1989: Transients and the extratropical response to El Niño. *J. Atmos. Sci.*, **46**, 163–174.

- Hendon, H. H., and M. L. Salby, 1994: The life cycle of the Madden–Julian Oscillation. *J. Atmos. Sci.*, **51**, 2225–2237.
- Hendon, H. H., D. W. J. Thompson, M. C. Wheeler, 2007: Australian rainfall and surface temperature variations associated with the Southern Hemisphere Annular Mode. *J. Climate*, **20**, 2452–2467.
- Hildebrandsson, H. H., 1897: Quelques recherches sur les entres d’action de l’atmosphère. *Kon. Svenska Vetens.-Akad. Handl.*, **29**, 33 pp.
- Horel, J. D., and J. M. Wallace, 1981: Planetary-scale atmospheric phenomena associated with the Southern Oscillation. *Mon. Wea. Rev.*, **109**, 813–829.
- Hoskins, B. J., and D. J. Karoly, 1981: The steady linear response of a spherical atmosphere to thermal and orographic forcing. *J. Atmos. Sci.*, **38**, 1179–1196.
- Houze, R. A., B. F. Smull, P. Dodge, 1990: Mesoscale organization of springtime rainstorms in Oklahoma. *Mon. Wea. Rev.*, **118**, 613–654.
- James, J., 1992: A preliminary study of mesoscale convective complexes over the mid-latitudes of eastern Australia. Technical Report 66, Bureau of Meteorology: Melbourne, 30 pp.
- Jirak, I. L., W. R. Cotton, R. L. McAnelly, 2003: Satellite and radar survey of mesoscale convective system development. *Mon. Wea. Rev.*, **131**, 2428–2449.
- Kharin, V. V., and F. W. Zwiers, 2005: Estimating extremes in transient climate change simulations. *J. Climate*, **18**, 1156–1173.
- Kharin, V. V., F. W. Zwiers, X. Zhang, G. C. Hegerl, 2007: Changes in temperature and precipitation extremes in the IPCC ensemble of global coupled model simulations. *J. Climate*, **20**, 1419–1444.
- Laing, A. G., 1992: Mesoscale convective complexes over Africa and Indian subcontinent. M. S. thesis, The Pennsylvania State University.
- Laing, A. G., and J. M. Fritsch, 1993a: Mesoscale convective complexes in Africa. *Mon.*

- Wea. Rev.*, **121**, 2254–2263.
- , and ——, 1993b: Mesoscale convective complexes over the Indian monsoon region. *J. Climate*, **6**, 911–919.
- , and ——, 1997: The global population of mesoscale convective complexes. *Quart J. Roy. Meteor. Soc.*, **123**, 389–405.
- Laing, A. G., J. M. Fritsch, A. J. Negri, 1999: Contribution of mesoscale convective complexes to rainfall in Sahelian Africa: Estimates from geostationary infrared and passive microwave data. *J. Appl. Meteor.*, **38**, 957–964.
- Laing, A. G., and J. M. Fritsch, 2000: The large-scale environments of the global populations of mesoscale convective complexes. *Mon. Wea. Rev.*, **128**, 2756–2776.
- Lau, K.-M., and P. J. Sheu, 1988: Annual Cycle, Quasi-Biennial Oscillation, and Southern Oscillation in Global Precipitation. *J. Geophys. Res.*, **93**, 10,975–10,988.
- Lorenz, E. N., 1951: Seasonal and irregular variations of the Northern Hemisphere sea-level pressure profile. *J. Meteor.*, **8**, 52–59.
- Machado, L. A. T., W. B. Rossow, R. L. Guedes, and A. W. Walker, 1998: Life cycle variations of mesoscale convective systems over the Americas. *Mon. Wea. Rev.* **126**: 1630–1654.
- Madden, R. A., and P. R. Julian, 1971: Detection of a 40–50 day oscillation in the zonal wind in the tropical Pacific. *J. Atmos. Sci.*, **28**, 702–708.
- Maddox, R. A., 1980: Mesoscale convective complexes. *Bul. Am. Met. Soc.*, **61**, 1374–1387.
- Mathon, V., H. Laurent, T. Lebel, 2002: Mesoscale convective system rainfall in the Sahel. *J. Appl. Meteor.*, **41**, 1081–1092.
- McAnelly, R. L., and W. R. Cotton, 1989: The precipitation life cycle of mesoscale convective complexes over the central United States. *Mon. Wea. Rev.*, **117**, 784–808.



- Mechoso, R. C., P. S. Días, W. Baetghen, V. Barros, E. H. Berbery, R. Clarke, H. Cullen, C. Ereño, B. Grassi, and D. Lettenmaier, 2001: *Climatology and Hydrology of the La Plata Basin*. Document of VAMOS/CLIVAR. 56. Available online: [http://www.atmos.umd.edu/~berbery/lpb/science\\_plan.html](http://www.atmos.umd.edu/~berbery/lpb/science_plan.html).
- Miller, D., and J. M. Fritsch, 1991: Mesoscale convective complexes in the western Pacific region. *Mon. Wea. Rev.*, **119**, 2978–2992.
- Mo, K. C., and G. H. White, 1985: Teleconnections in the Southern Hemisphere. *Mon. Wea. Rev.*, **113**, 22–37.
- Mota, G. V., 2003: Characteristics of rainfall and precipitation features defined by the Tropical Rainfall Measuring Mission over South America. Ph.D. dissertation, University of Utah, 215 pp.
- National Research Council, Climate Research Committee, Board on Atmospheric Sciences and Climate, Commission on Physical Sciences, Mathematics and Resources, 1983: El Niño and the Southern Oscillation: A scientific plan. 72 pp.
- Ferreira, R. N., T. M. Rickenbach, D. L. Herdies, and L. M. V. Carvalho, 2003: Variability of South American convective cloud systems and tropospheric circulation during January–March 1998 and 1999. *Mon. Wea. Rev.*, **131**, 961–973.
- Pisciottano, G., A. Díaz, G. Cazes, C. R. Mechoso, 1994: El Niño – Southern Oscillation impact on rainfall in Uruguay. *J. Climate*, **7**, 1286-1302.
- Rao, V. B., and K. Hada, 1990: Characteristics of rainfall over Brazil: Annual variations and connections with the Southern Oscillation. *Theor. Appl. Climatol.*, **42**, 81-91.
- Reason, C. J. C., and M. Rouault, 2005: Links between the Antarctic Oscillation and winter rainfall over western South Africa. *Geophys. Res. Lett.*, **32**, L07705, 4 pp.
- Reboita, M. S., T. Ambrizzi, R. P. da Rocha, 2009: Relationship between the Southern Annular Mode and Southern Hemisphere atmospheric systems. *Revista Brasileira de Meteorologia*, **24**, 48-55.
- Rodgers, D. M., K. W. Howard, E. C. Johnson, 1983: Mesoscale convective complexes

- over the United States during 1982. *Mon. Wea. Rev.*, **111**, 2363-2369.
- Rogers, J. C., and H. Van Loon, 1982: Spatial variability of sea level pressure and 500 mb height anomalies over the Southern Hemisphere. *Mon. Wea. Rev.*, **110**, 1375-1392.
- Ropelewski, C. F., and M. S. Halpert, 1987: Global and regional scale precipitation patterns associated with the El Niño / Southern Oscillation. *Mon. Wea. Rev.*, **115**, 1606-1626.
- Ropelewski, C. F., and M. S. Halpert, 1989: Precipitation patterns associated with the high index phase of the Southern Oscillation. *J. Climate*, **2**, 268-284.
- Ropelewski, C. F., and M. S. Halpert, 1996: Quantifying Southern Oscillation – precipitation relationships. *J. Climate*, **9**, 1043-1059.
- Salio, P., M. Nicolini, E. J. Zipser, 2007: Mesoscale convective systems over southeastern South America and their relationship with the South American low-level jet. *Mon. Wea. Rev.*, **135**, 1290–1309.
- Silvestri, G. E., and C. S. Vera, 2003: Antarctic Oscillation signal on precipitation anomalies over southeastern South America. *Geophys. Res. Lett.*, **30**, CLM 3.1-CLM 3.4.
- Thompson, D. W. J., and J. M. Wallace, 1998: The Arctic Oscillation signature in the wintertime geopotential height and temperature fields. *Geophys. Res. Lett.*, **25**, 1297-1300.
- Thompson, D. W. J., and J. M. Wallace, 2000: Annular Modes in the Extratropical Circulation. Part I: Month-to-Month Variability. *J. Climate*, **13**, 1000-1016.
- Tollerud, E. I. and R. S. Collander, 1993: Mesoscale convective systems and extreme rainfall in the central United States. Extreme Hydrological Events: Precipitation, Floods, and Droughts. *Hydrological Science*, **213**, 11-19.
- Trenberth, K. E., 1997: The definition of El Niño. *Bull. Amer. Meteor. Soc.*, **78**, 2771-2777.

- Trenberth, K. E., G. W. Branstator, D. Karoly, A. Kumar, N. Lau, C. Ropelewski, 1998: Progress during TOGA in understanding and modeling global teleconnections associated with tropical sea surface temperatures. *J. Geophys. Res.*, **103**, 14,291-14,324.
- Velasco, I., and J. M. Fritsch, 1987: Mesoscale convective complexes in the Americas. *J. Geophys. Res.*, **92**, 9591–9613.
- Vera, C., and Coauthors, 2006: The South American low-level jet experiment. *Bull. Amer. Meteor. Soc.*, **87**, 63–77.
- Viana, D. R., 2006: Avaliação da precipitação e desastres naturais associados a complexos convectivos de mesoescala no Rio Grande do Sul entre Outubro e Dezembro de 2003. M.S. thesis, Departamento de Geografia, Universidade Federal do Rio Grande Do Sul, 136 pp.
- Visbeck, Martin, 2009: A station-based southern annular mode index from 1884 to 2005. *J. Climate*, **22**, 940–950.
- Walker, G. T., and E. W. Bliss, 1932: World Weather V. *Mem. Roy. Meteor. Soc.*, **4**, 53-84.
- Wallace, J. M., and D. S. Gutzler, 1981: Teleconnections in the geopotential height field during the Northern Hemisphere winter. *Mon. Wea. Rev.*, **109**, 784–812.
- Wehner, M. F., 2004: Predicted twenty-first-century changes in seasonal extreme precipitation events in the parallel climate model. *J. Climate*, **17**, 4281–4290.

APPENDIX A: TABLES

**Table 1.** Mesoscale Convective Complex definition established by Maddox (1980), with cloud top temperature modification described by Augustine and Howard (1988).

<b>Mesoscale Convective Complex (MCC) and Persistent Elongated Convective System (PECS) Characteristics</b>	
<b>Size:</b>	Interior cold–cloud region with temperature of $-52\text{ }^{\circ}\text{C}$ must have an area of $50\,000\text{ km}^2$
<b>Initiation:</b>	Size definition first satisfied
<b>Duration:</b>	Size definition must be met for $\geq 6$ hours
<b>Maximum Extent:</b>	Contiguous cold–cloud shield (IR temperature $-52\text{ }^{\circ}\text{C}$ ) reaches maximum size
<b>Shape:</b>	<b>MCCs:</b> Eccentricity (minor axis/major axis) $\geq 0.7$ at time of maximum extent  <b>PECS:</b> $0.2 < \text{Eccentricity} < 0.7$ at time of maximum extent
<b>Termination:</b>	Size definition no longer satisfied

**Table 2.** Frequency of LLCs occurrence over combinations of monthly ENSO and daily AAO phases.

	<b>ENSO +, AAO +</b>	<b>ENSO +, AAO neutral</b>	<b>ENSO +, AAO -</b>	<b>ENSO neutral, AAO +</b>	<b>ENSO neutral, AAO neutral</b>	<b>ENSO neutral, AAO -</b>	<b>ENSO -, AAO +</b>	<b>ENSO -, AAO neutral</b>	<b>ENSO -, AAO -</b>
<b>Number of LLCs</b>	24	342	102	89	456	104	85	360	55
<b>Number of days in POR</b>	25	330	103	145	797	120	149	455	65
<b>Number of LLCs/Day</b>	0.96	1.04	0.99	0.61	0.57	0.87	0.57	0.79	0.85

**Table 3.** Independent-sample t-tests for difference of means between negative (-), neutral (=), and positive (+) AAO phases under negative, neutral and positive ENSO conditions. Symbols in parentheses indicate the phase of the AAO for which the mean of each variable is valid, with the value on the right subtracted from the value on the left in each case. Statistically significant p-values at the 95% confidence level are in bold.

LLCS characteristic and AAO phases	NEGATIVE ENSO PHASES		NEUTRAL ENSO PHASES		POSITIVE ENSO PHASES	
	Difference in means, 95% conf. int.	P-value	Difference in means, 95% conf. int.	P-value	Difference in means, 95% conf. int.	P-value
Max. Area: (-)=(=)	15621.82, 139005.69	<b>0.0148</b>	-69090.96, -2458.32	<b>0.0354</b>	-19730.13, 89668.87	0.2085
Max. Area: (-)(+)	23136.39, 164648.37	<b>0.0098</b>	-59526.56, 37556.50	0.6555	-228.57, 160941.12	0.0506
Max. Area: (=)(+)	-26917.63, 60074.88	0.452	-19861.14, 69440.36	0.2741	-23313.99, 114087.80	0.1873
Latitude: (-)=(=)	-1.756058, 3.012874	0.6036	-2.664, 0.418	0.1519	-4.012, -0.727	<b>0.005</b>
Latitude: (-)(+)	-0.927, 3.806	0.2309	-4.930, -0.811	<b>0.0066</b>	-6.325, 0.676	0.1102
Latitude: (=)(+)	-1.491, 3.114	0.4885	-3.434, -0.061	<b>0.0424</b>	-3.764, 2.854	0.7795
Duration: (-)=(=)	-0.998, 4.962	0.189	-4.031, 1.703	0.4236	-1.788, 4.317	0.4144
Duration: (-)(+)	-3.749, 4.536	0.8512	-4.083, 3.928	0.9696	-6.695, 7.776	0.88
Duration: (=)(+)	-4.841, 1.664	0.3351	-2.169, 4.343	0.5099	-7.600, 6.152	0.8301
Eccentricity: (-)=(=)	-0.078, 0.020	0.239	-0.021, 0.053	0.3899	-0.072, 0.004	0.0777
Eccentricity: (-)(+)	-0.084, 0.030	0.345	-0.078, 0.023	0.285	-0.087, 0.063	0.7487
Eccentricity: (=)(+)	-0.037, 0.041	0.9302	-0.085, -0.002	<b>0.0382</b>	-0.049, 0.093	0.5269

APPENDIX B: FIGURES

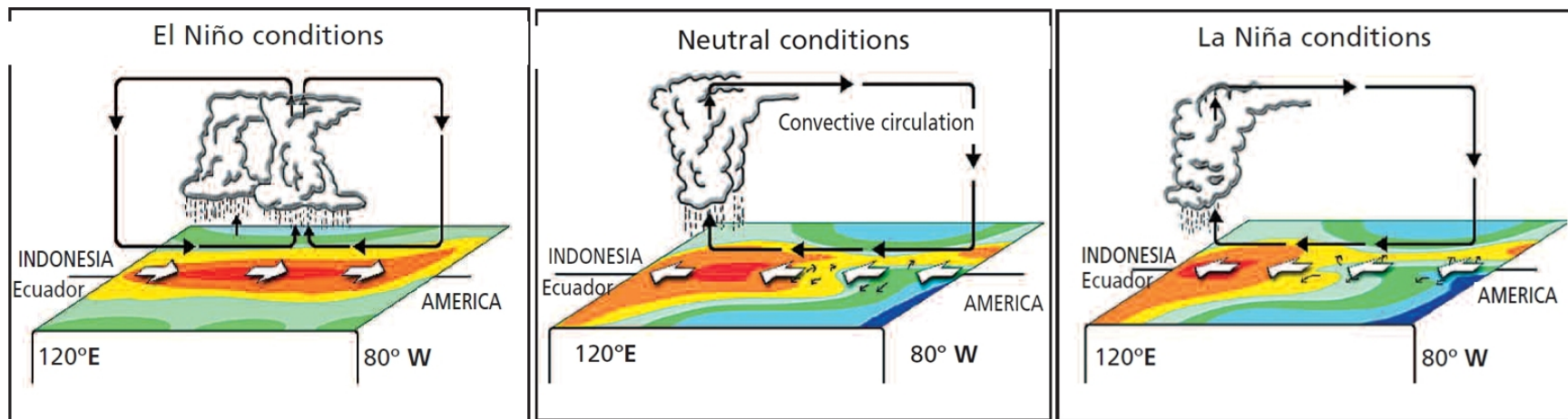


**Fig. 1.** From Ambrizzi (2006). 3-D view of ocean-atmosphere features in the equatorial Pacific during ENSO phases.

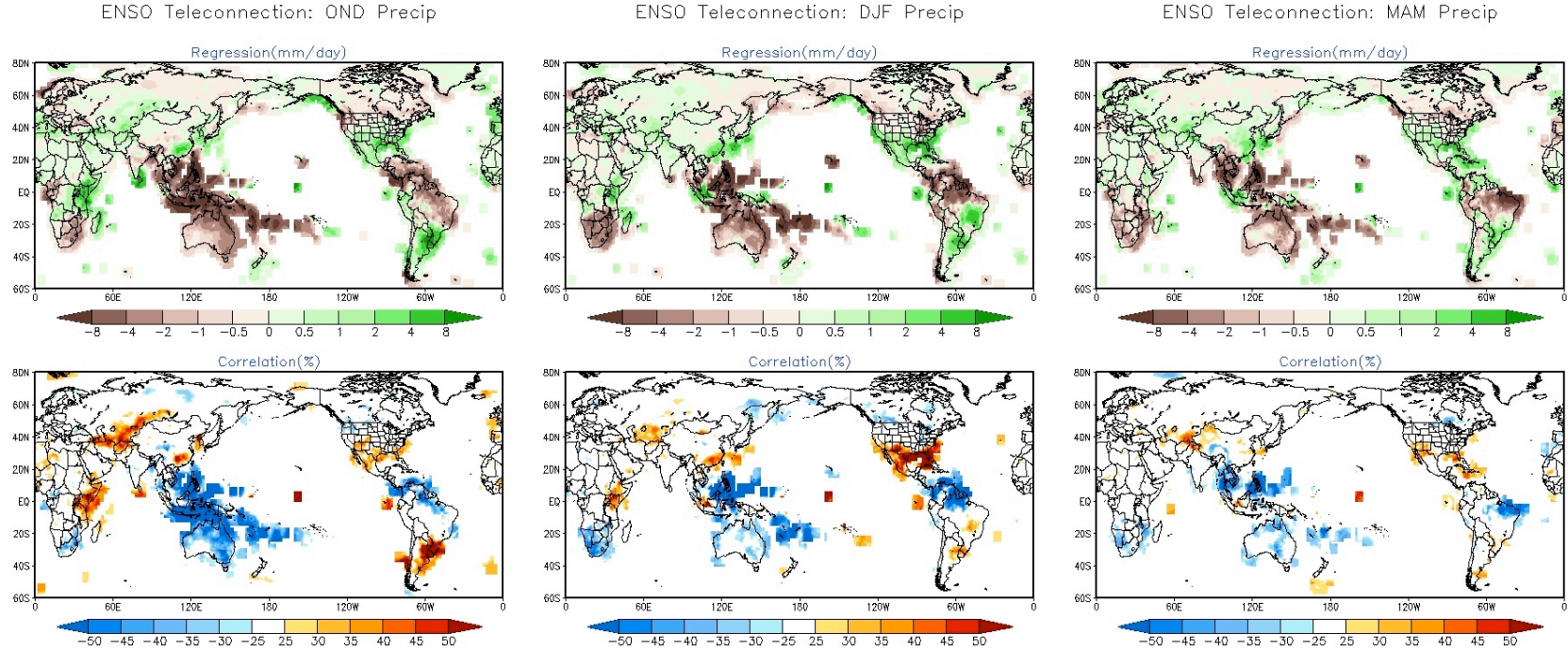


**Fig. 2.** From Climate Prediction Center (2012). Linear regression of ENSO index with global precipitation anomalies from the 1980-2010 mean (top) and correlations between ENSO index and precipitation anomalies (bottom) for October-November-December (left), December-January-February (middle), and March-April-May (right).



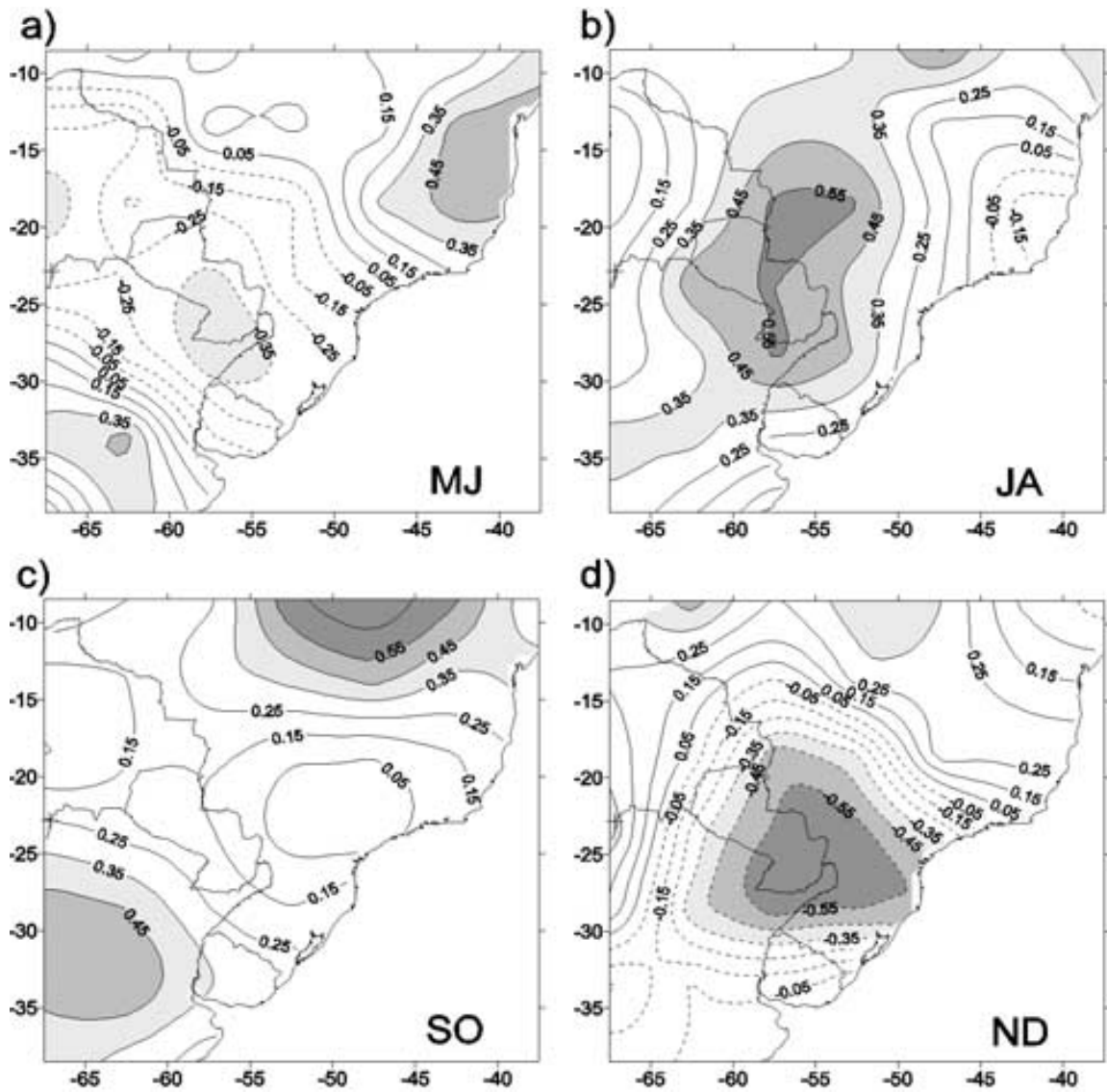


**Fig. 3.** From Silvestri and Vera (2003). Correlation maps between AAO index and bi-monthly precipitation anomalies over SSA for (a) May-June, (b) July-August, (c) September-October, and (d) November-December. Shadings indicate statistical significance at the 90, 95, and 99% confidence intervals. Smooth lines indicate positive correlations and dashed lines indicate negative correlations.

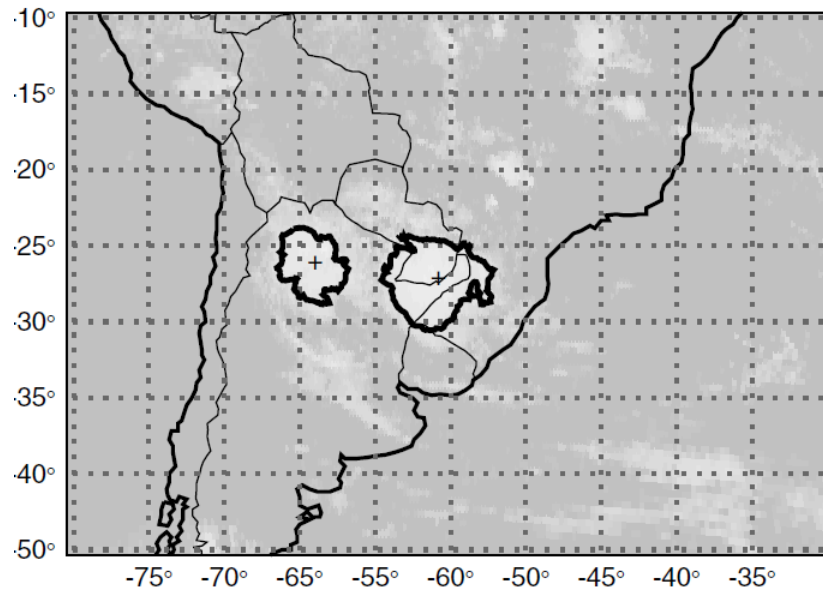
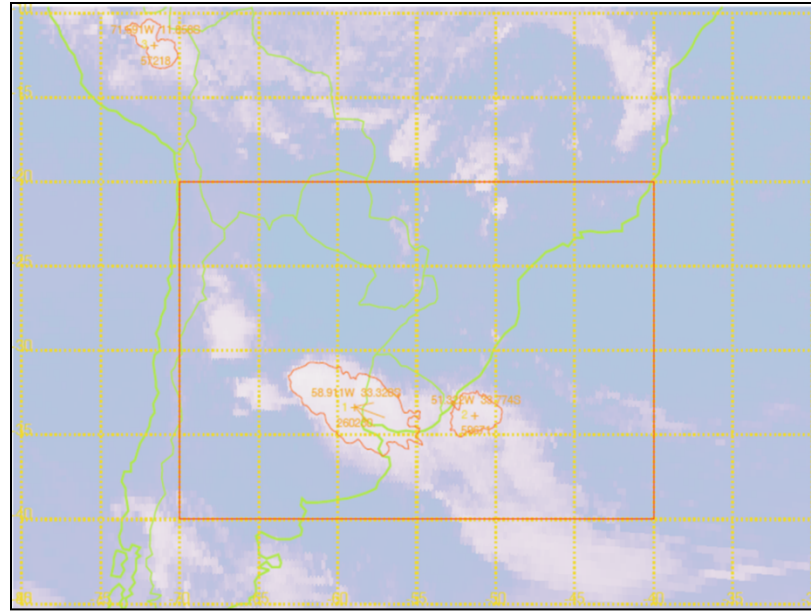


**Fig. 4.** Sample scenes of GOES imagery used to compile dataset, showing study domain of  $-70^{\circ}$  to  $-40^{\circ}$  W,  $20^{\circ}$  to  $40^{\circ}$  S. Bottom graphic is from DM09.

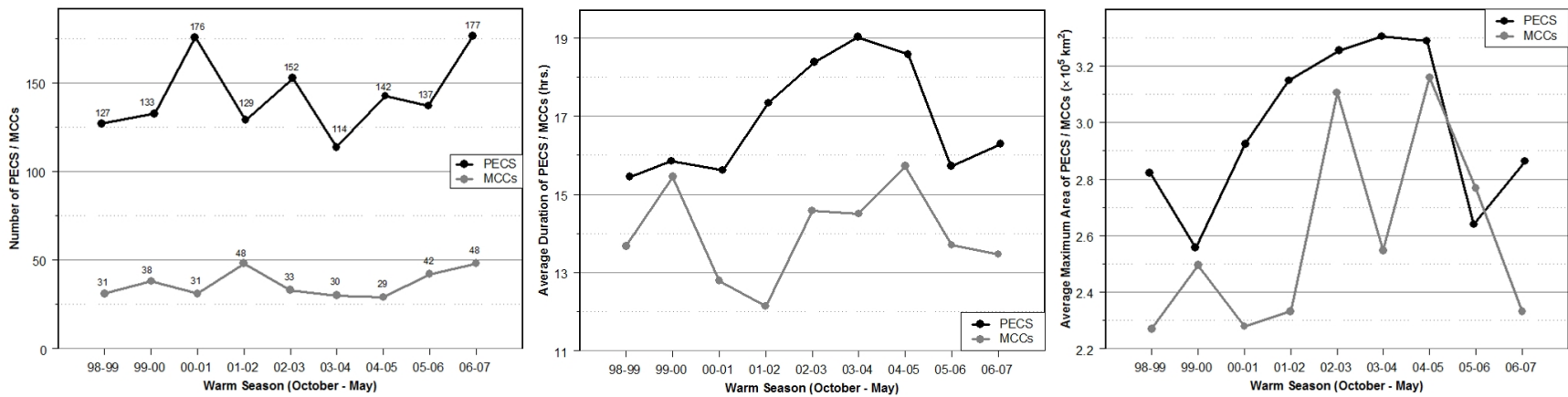


**Fig. 5.** Number of PECS and MCCs (a), average PECS and MCC duration (b), and average PECS and MCC maximum area (c) for each warm season.

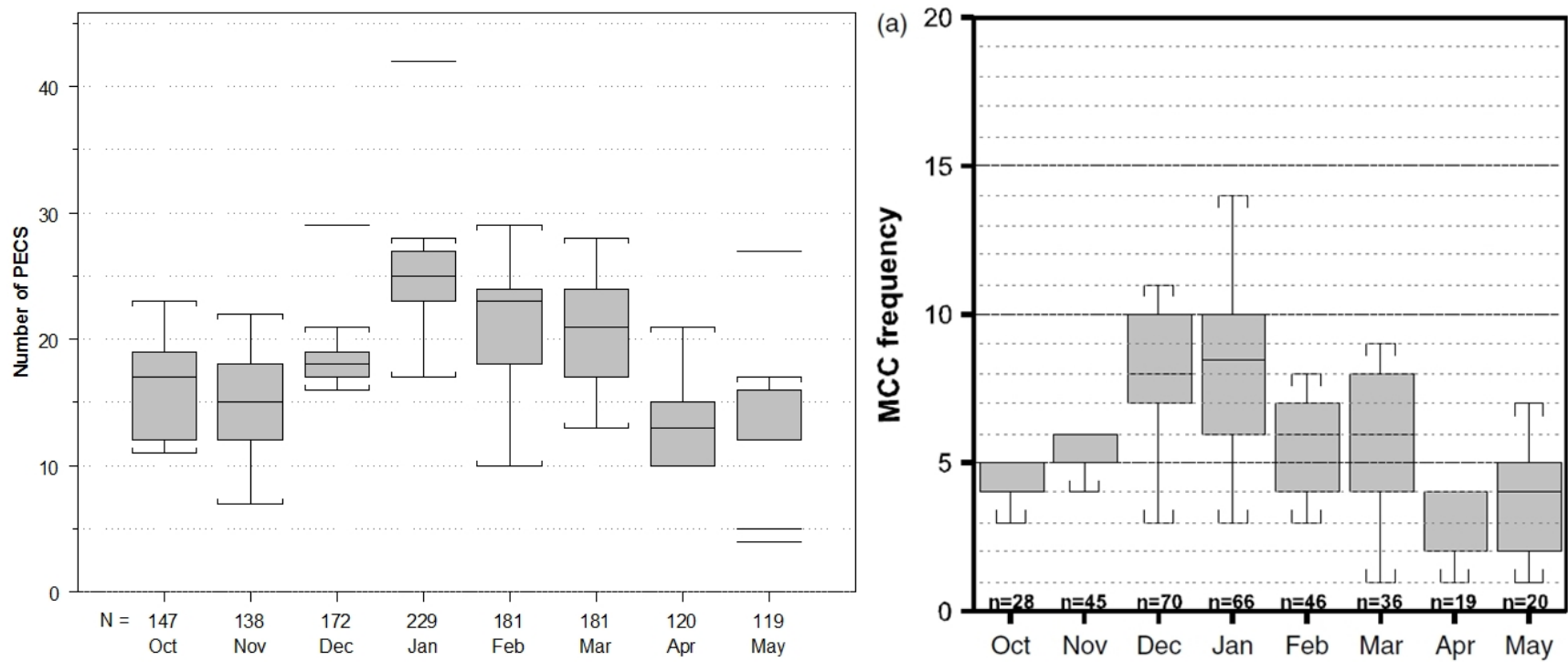


**Fig. 6.** Intraseasonal distribution of PECS (a) and MCCs (b, from DM09). On PECS graphic, whiskers extend to 1.5 times the interquartile range, with outliers denoted by horizontal lines. On MCC graphic, whiskers show the 10<sup>th</sup> and 90<sup>th</sup> percentiles.

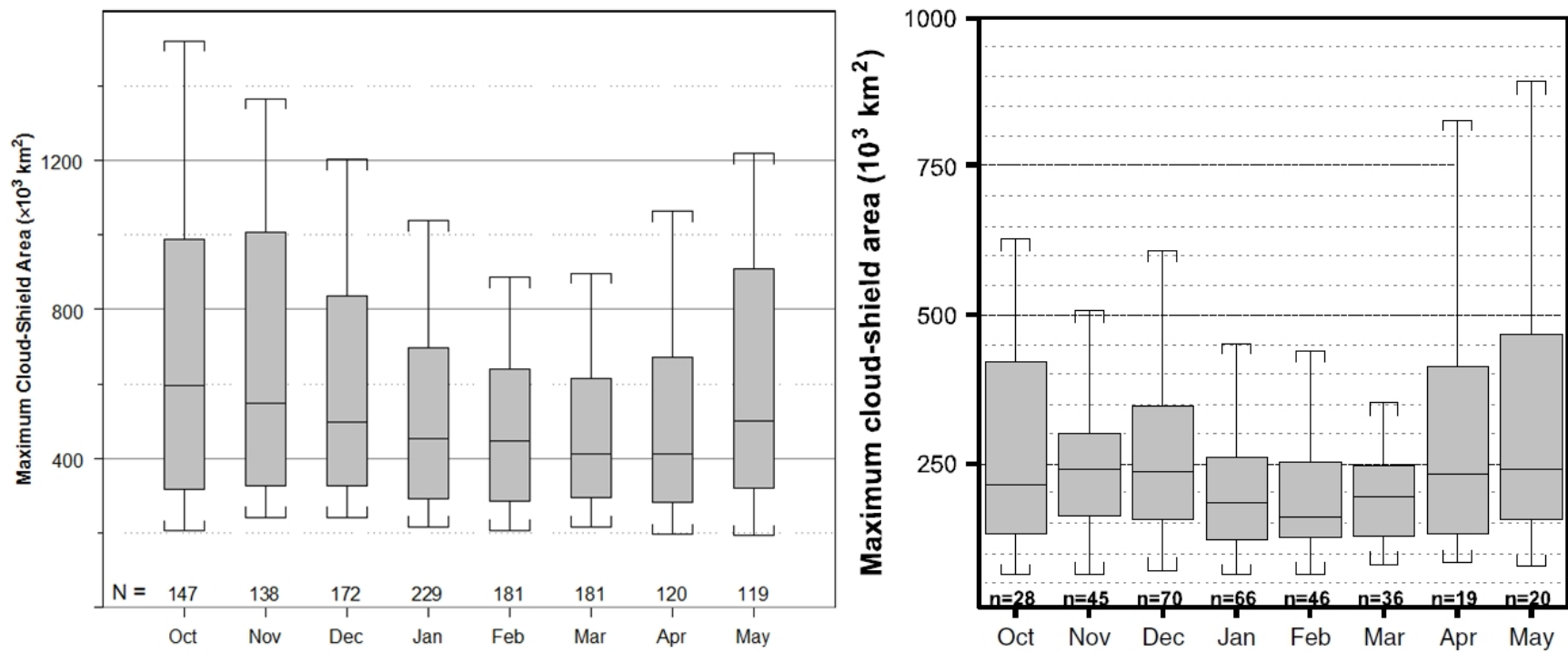


**Fig. 7.** Intraseasonal distribution of maximum <-52 °C cloud shield area attained by PECS (a) and MCCs (b, from DM09). Whiskers show the 10<sup>th</sup> and 90<sup>th</sup> percentiles.

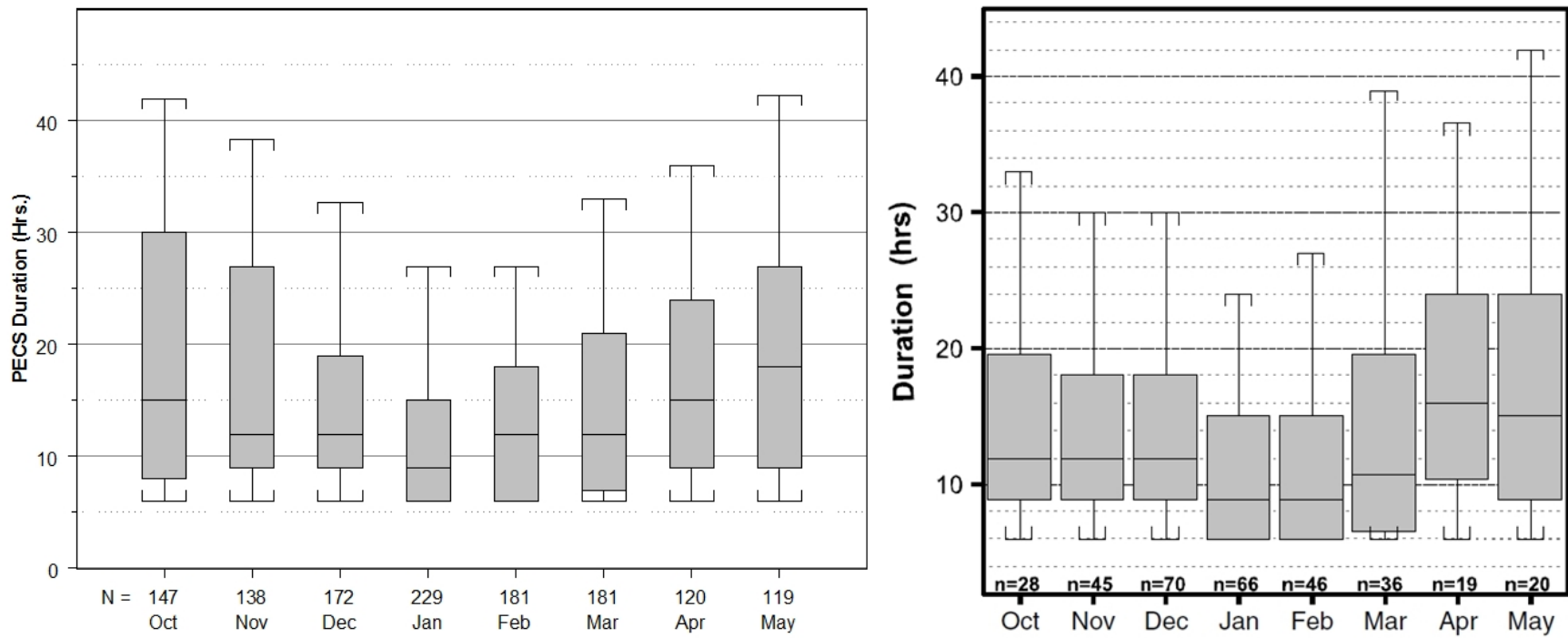


**Fig. 8.** Intraseasonal distribution of duration of PECS (a) and MCCs (b, from DM09). Whiskers show the 10<sup>th</sup> and 90<sup>th</sup> percentiles.

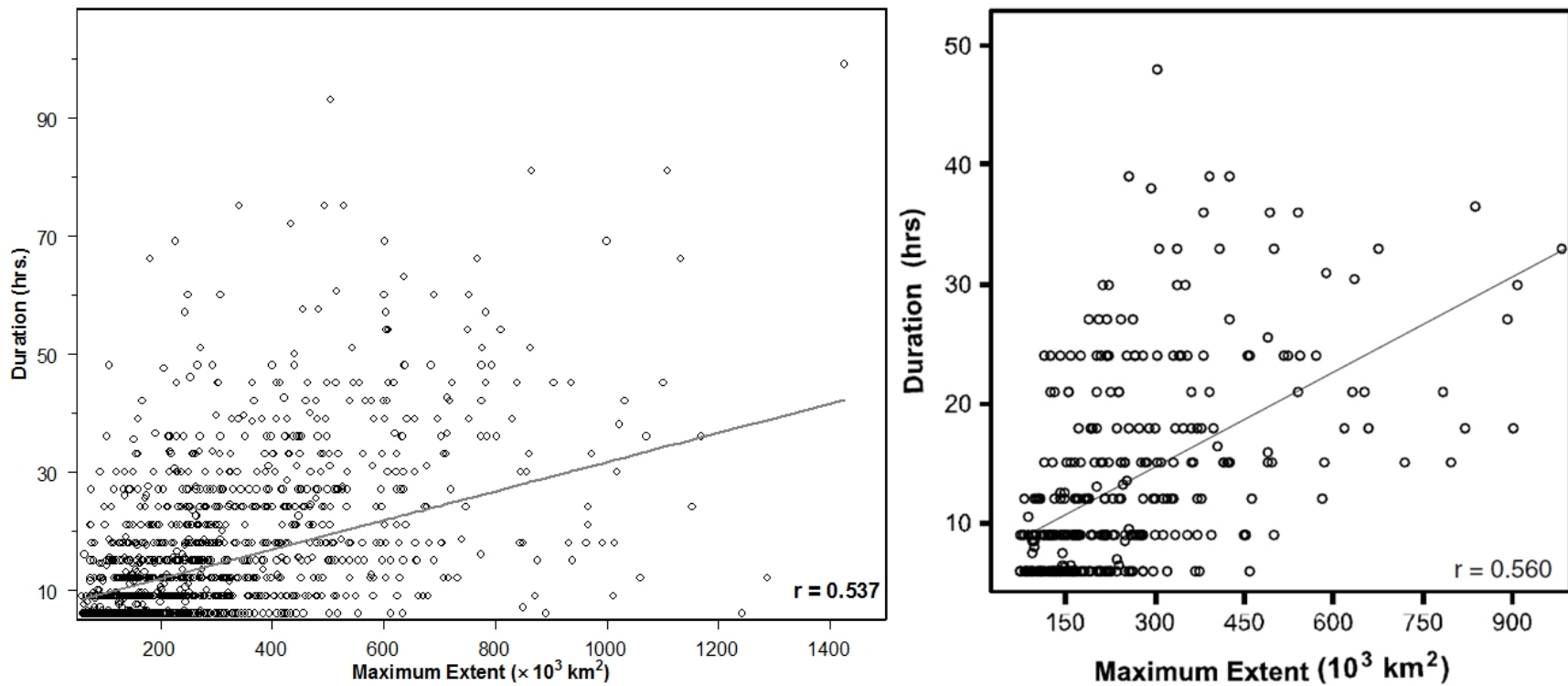


**Fig. 9.** Scatter plot showing relationship between duration and maximum extent for all PECS (a) and MCCs (b, from DM09).

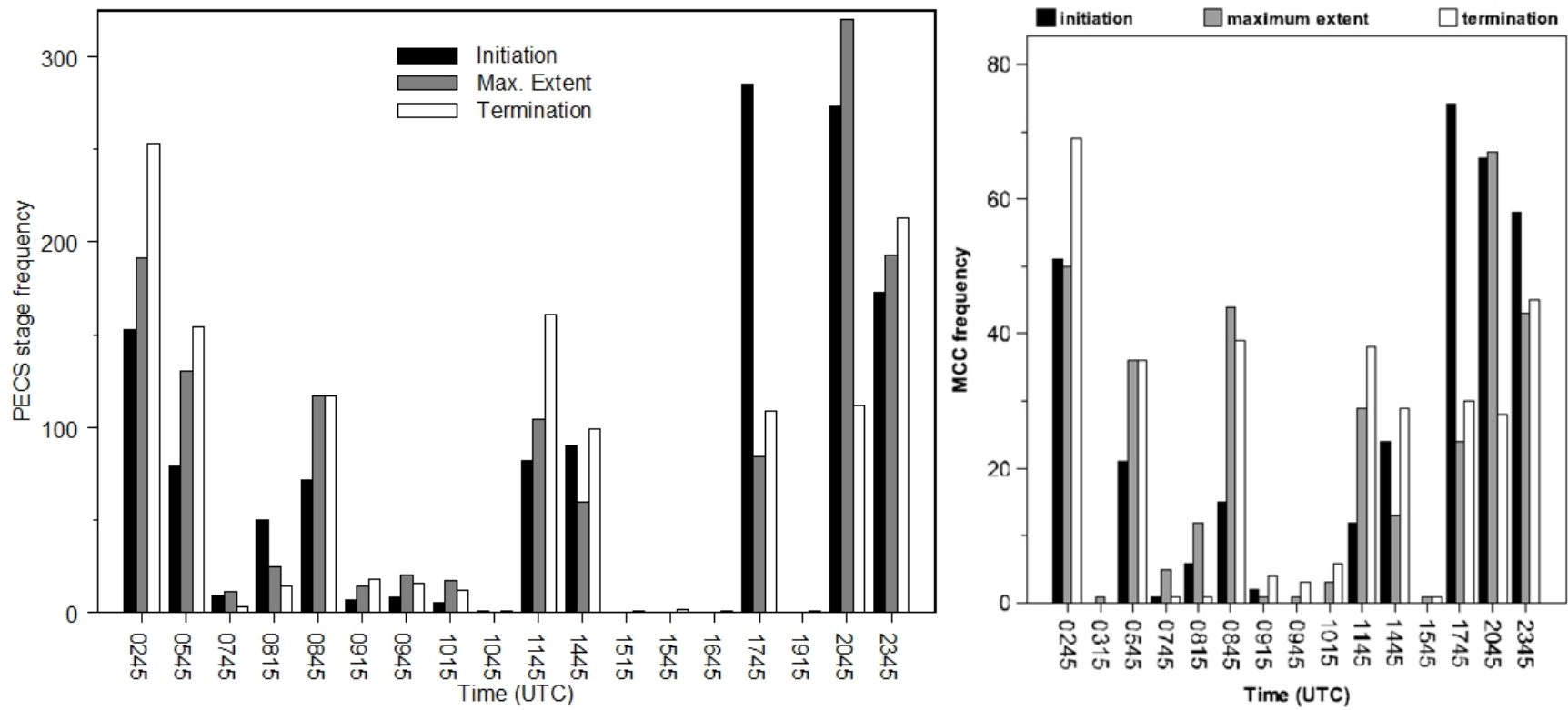


**Fig. 10.** Diurnal distribution of PECS (a) and MCCs (b, from DM09) critical stages.



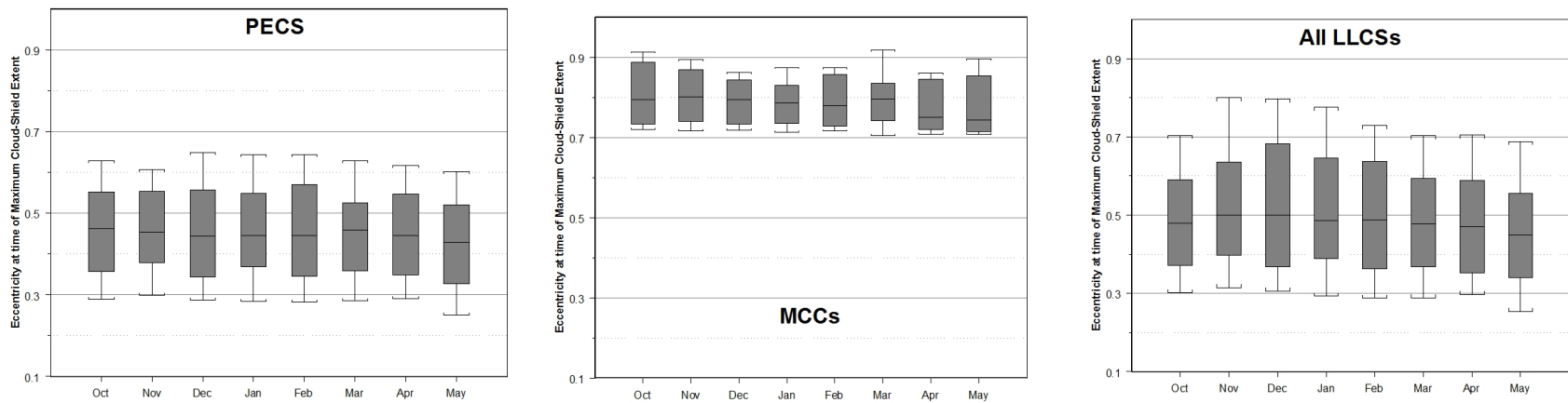


**Fig. 11.** Intraseasonal distribution of eccentricity of  $< -52$  °C cloud shields associated with PECS (a), MCCs (b), and all LLCs (c) at time of maximum extent. Whiskers show the 10<sup>th</sup> and 90<sup>th</sup> percentiles.

### Point Density of PECS at All Stages

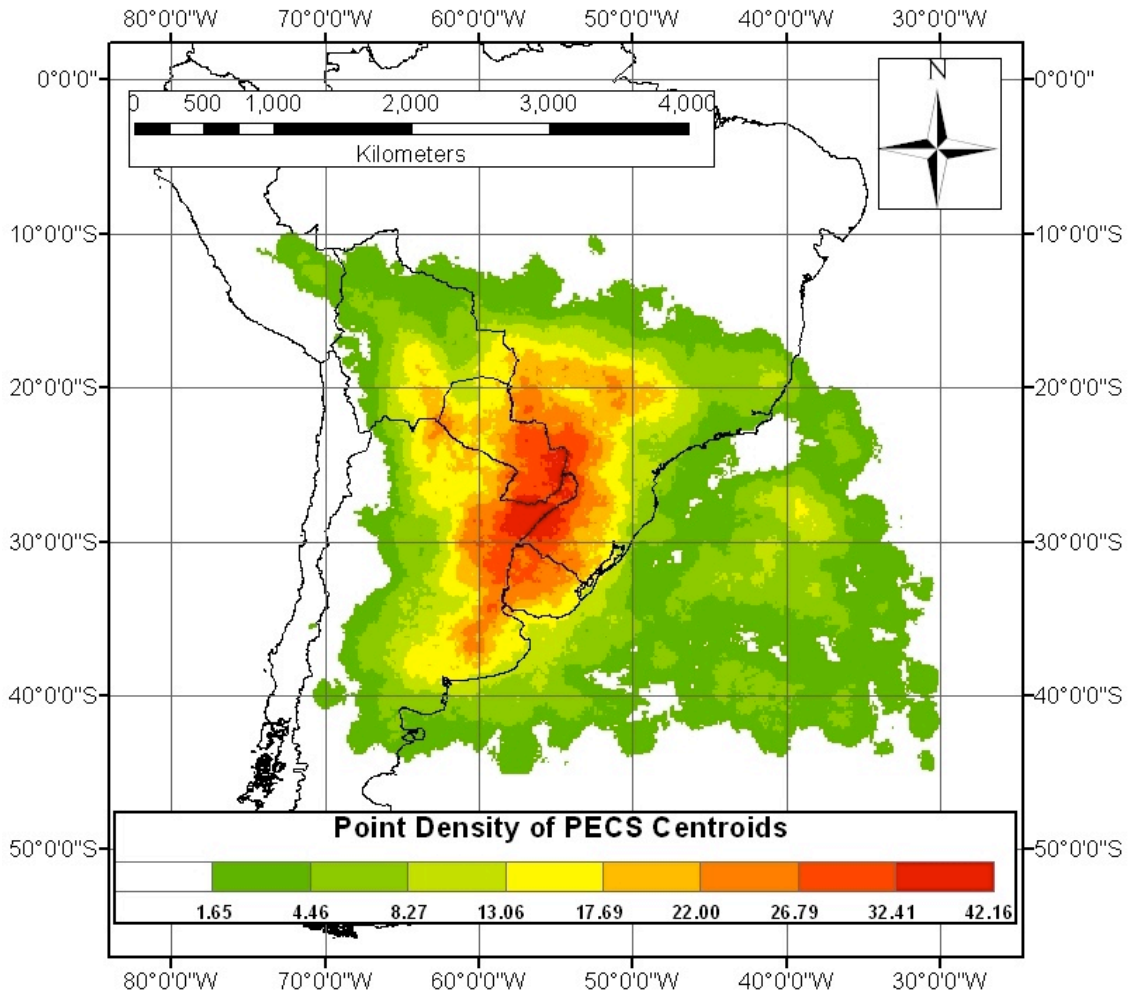


**Fig. 12.** Point density map showing location of all PECS centroids for the entire 1998-2007 study period.

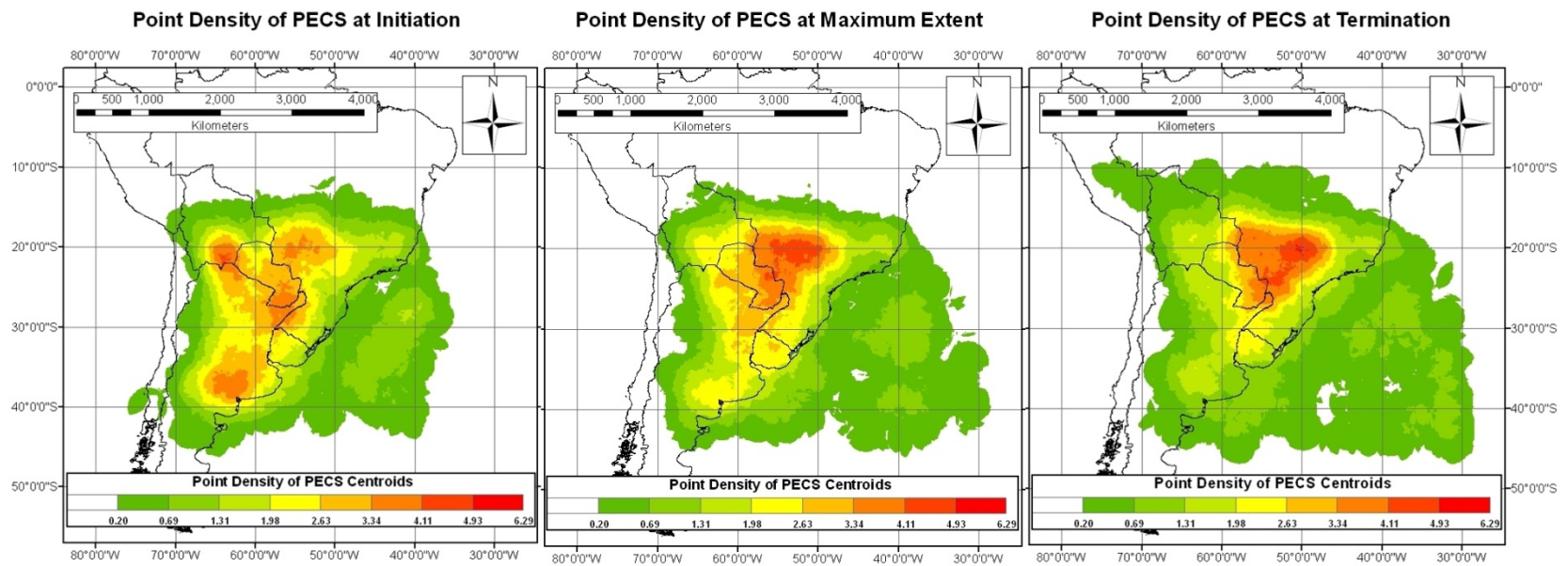


**Fig. 13.** Point density map showing locations of PECS centroids at time of initiation (a), maximum extent (b), and termination (c).

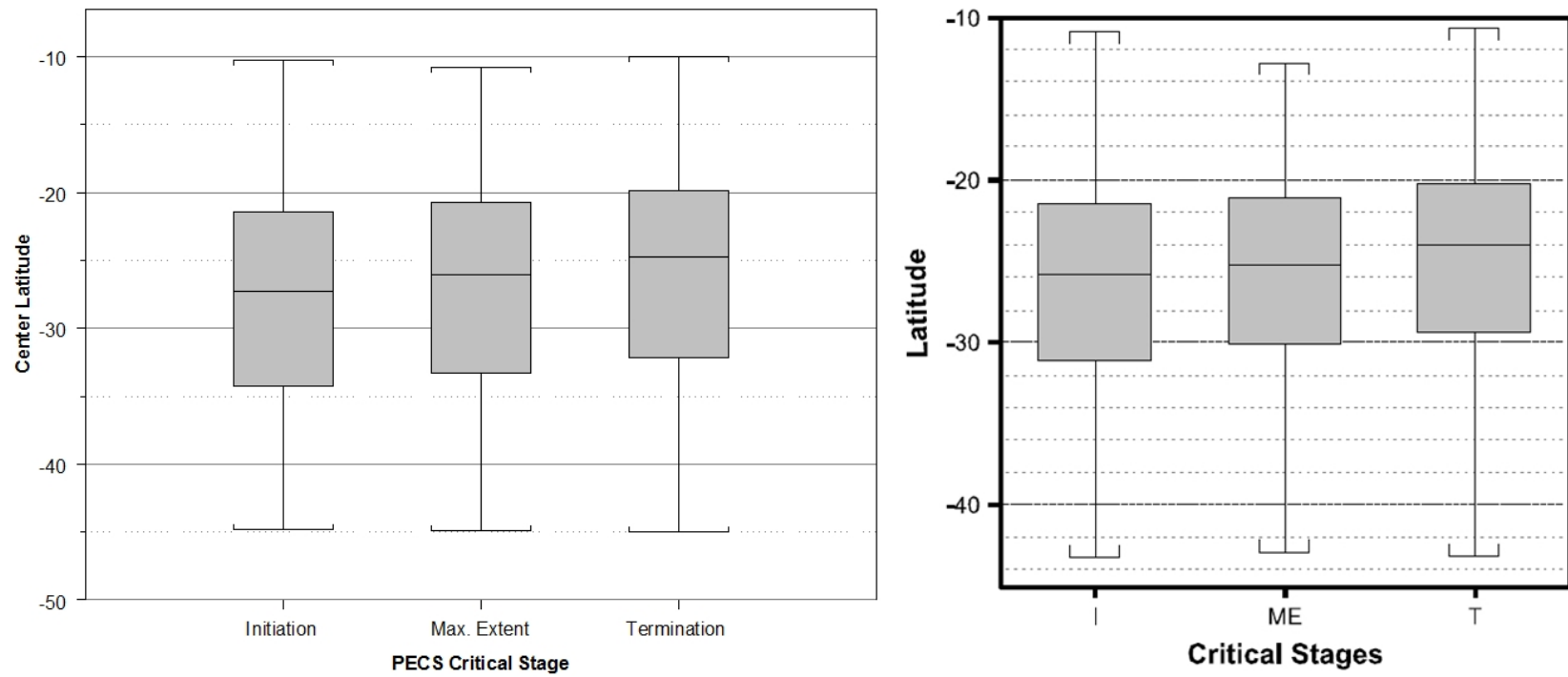


**Fig. 14.** Latitude of PECS (a) and MCC (b, from DM09) centroids at critical stages. Whiskers show the 10<sup>th</sup> and 90<sup>th</sup> percentiles.

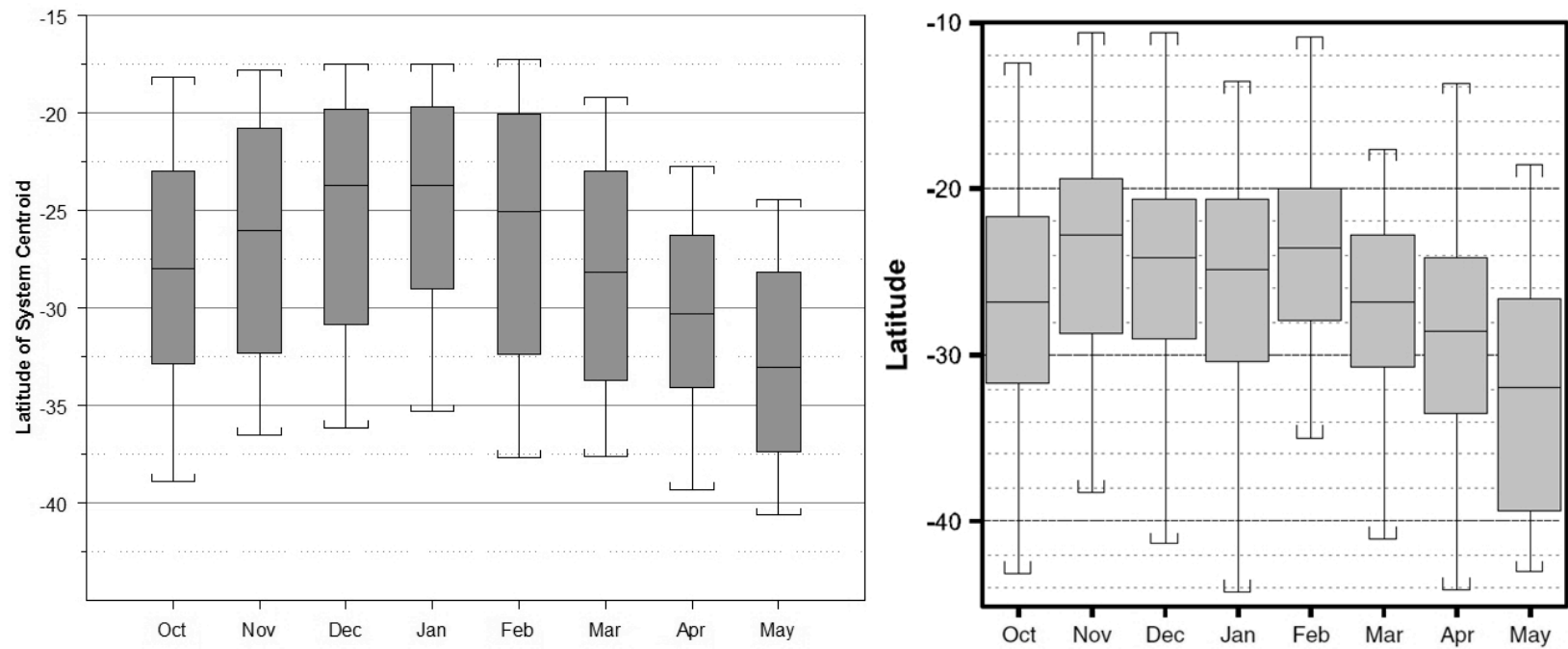


**Fig. 15.** Intraseasonal distribution of latitude of PECS (a) and MCC (b, from DM09) centroids at all points in their life cycle. Whiskers show the 10<sup>th</sup> and 90<sup>th</sup> percentiles.

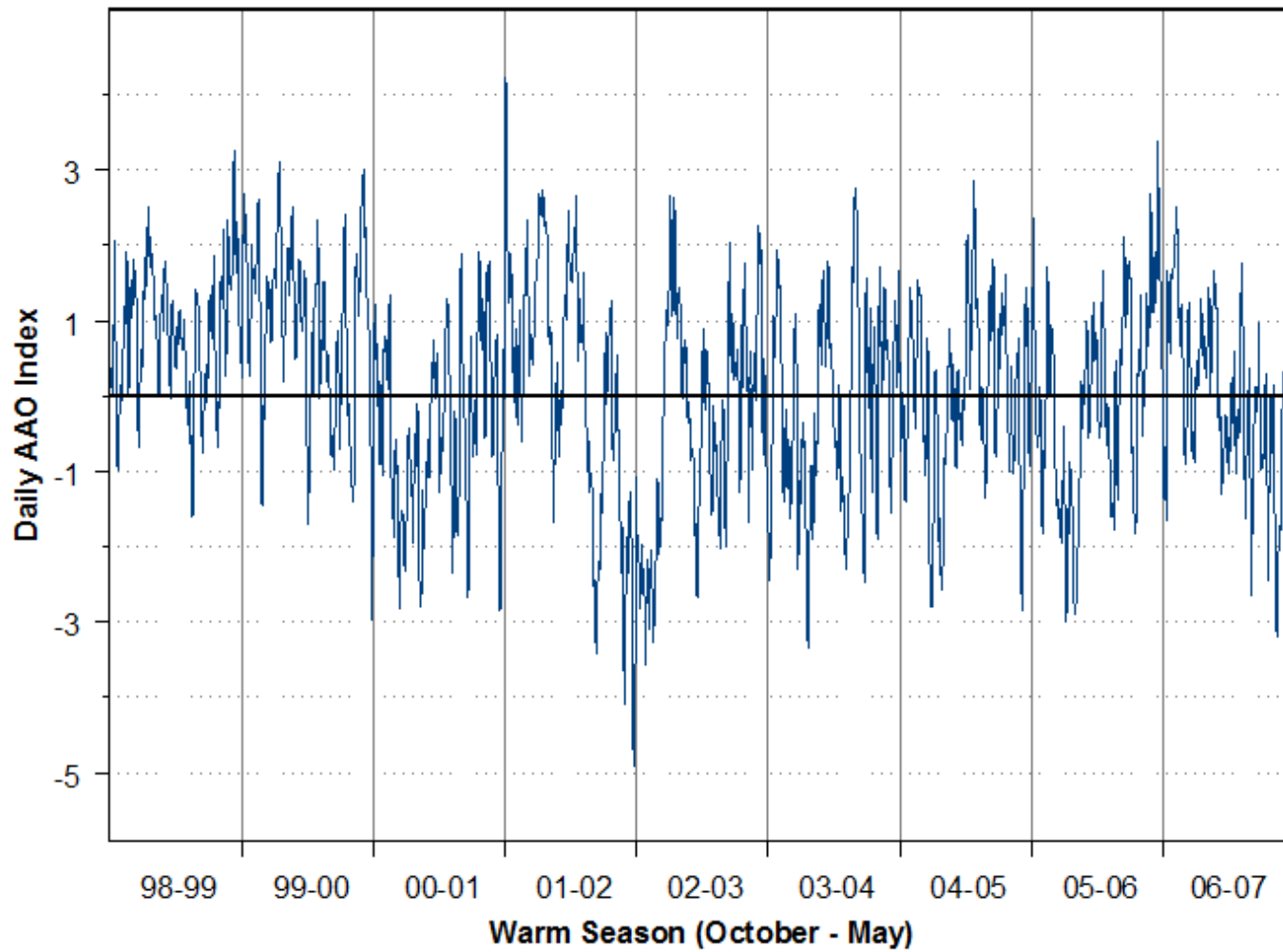


**Fig. 16.** Time series of daily AAO index for entire study period.

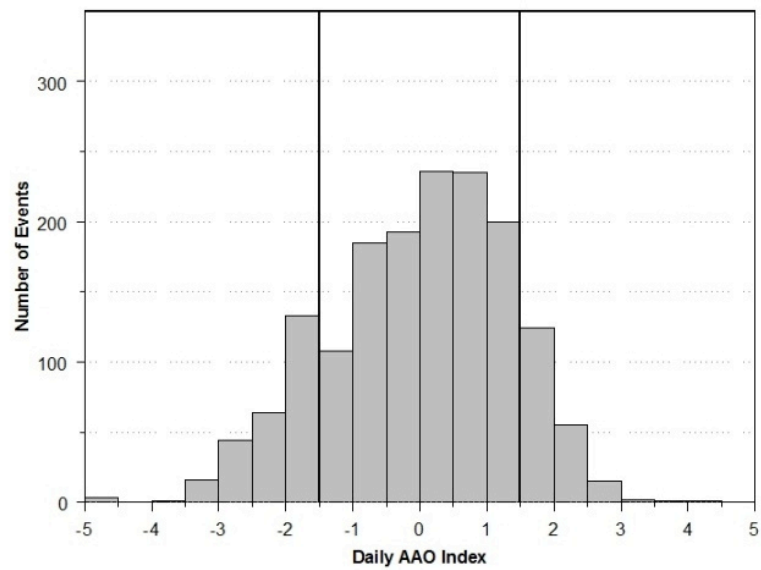
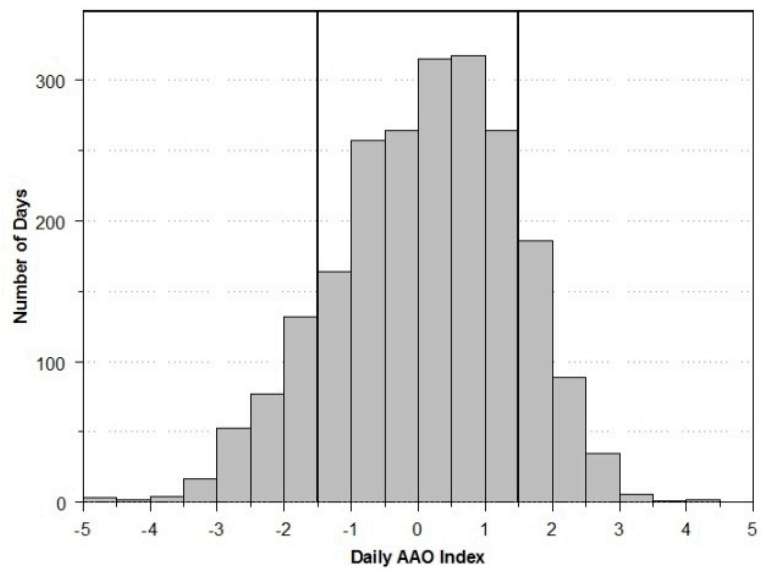


**Fig. 17.** Distribution of daily AAO index values for entire study period (a) and on days when an LLCS occurred (b).

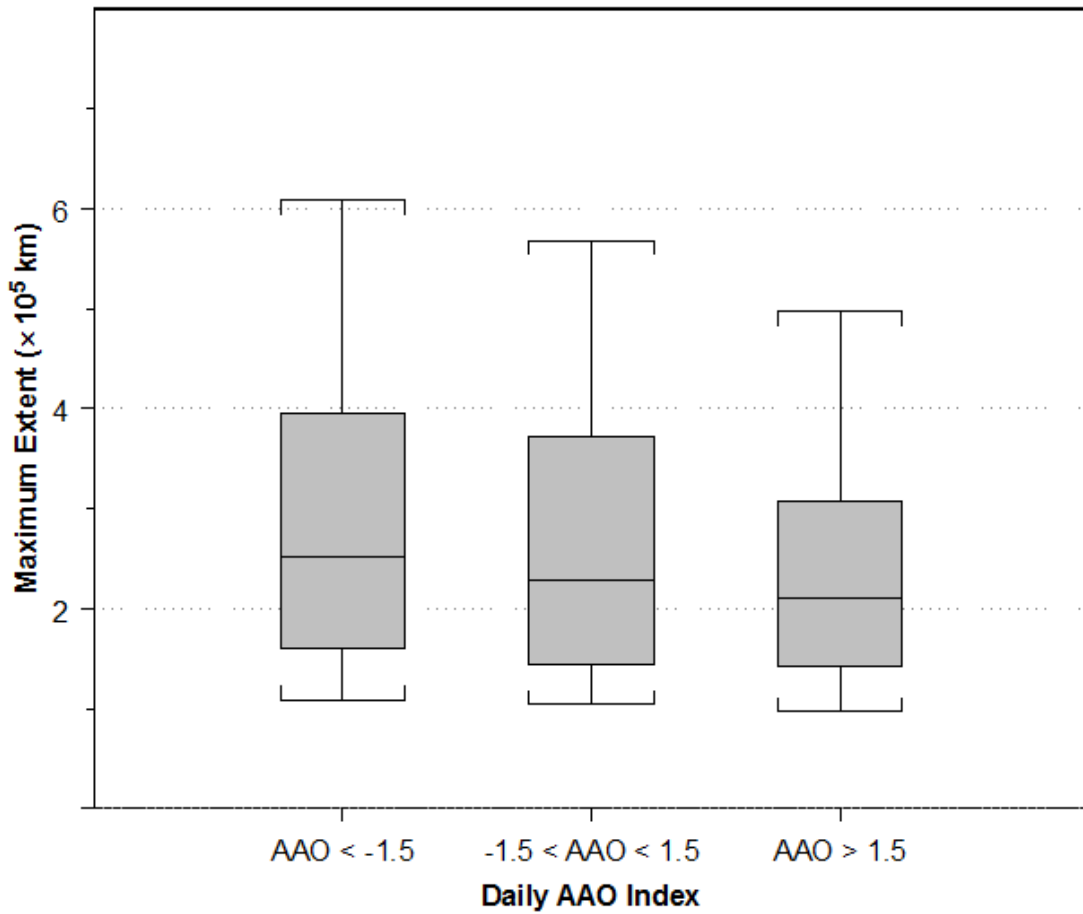


**Fig. 18.** Maximum extent reached by each LLCS during negative, neutral, and positive AAO phases. Whiskers show the 10<sup>th</sup> and 90<sup>th</sup> percentiles.



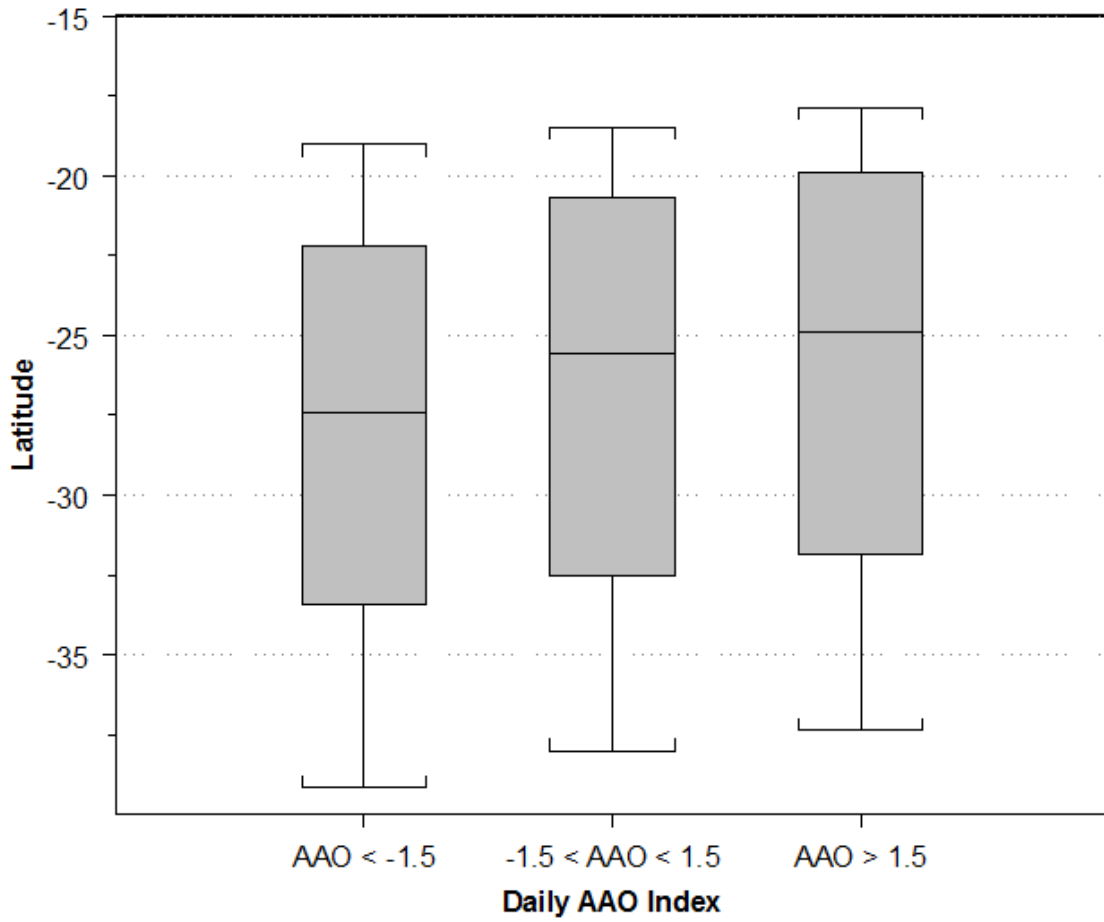


**Fig. 19.** As in fig. 15 except for the latitude of LLCS centroids at their maximum extent.

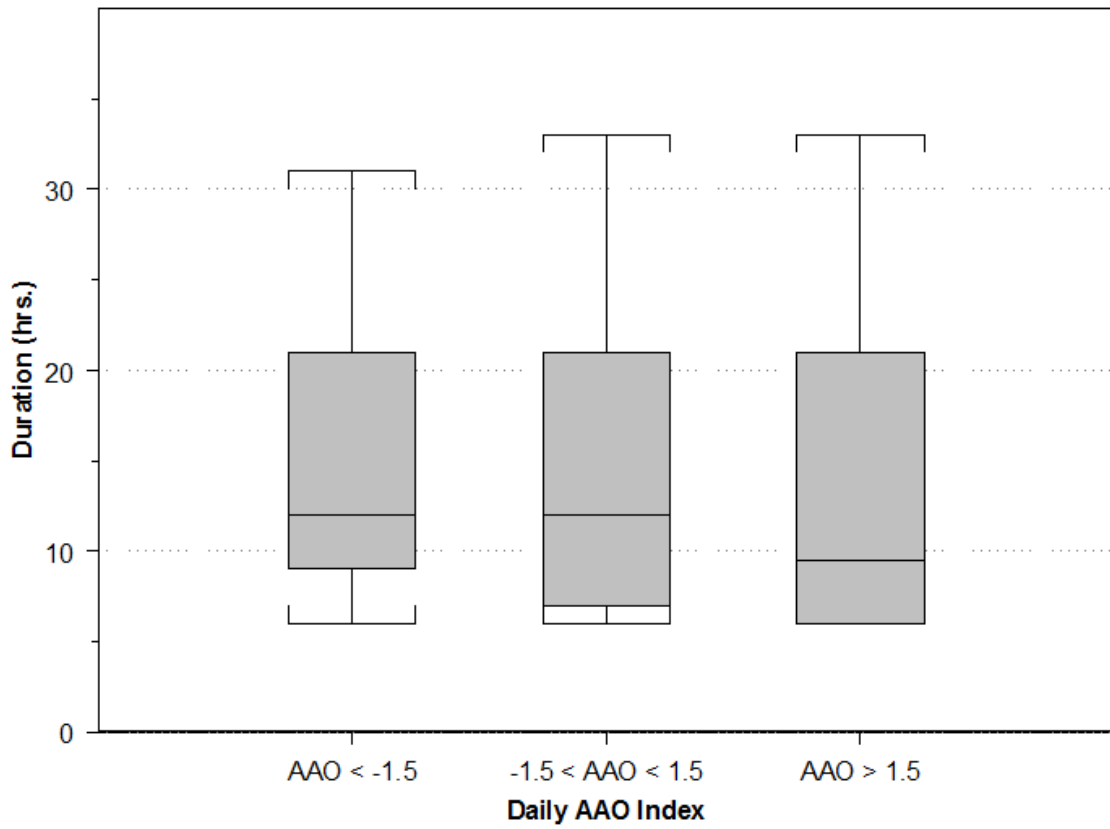


**Fig. 20.** As in figs. 15 and 16 except for the duration of LLCs.

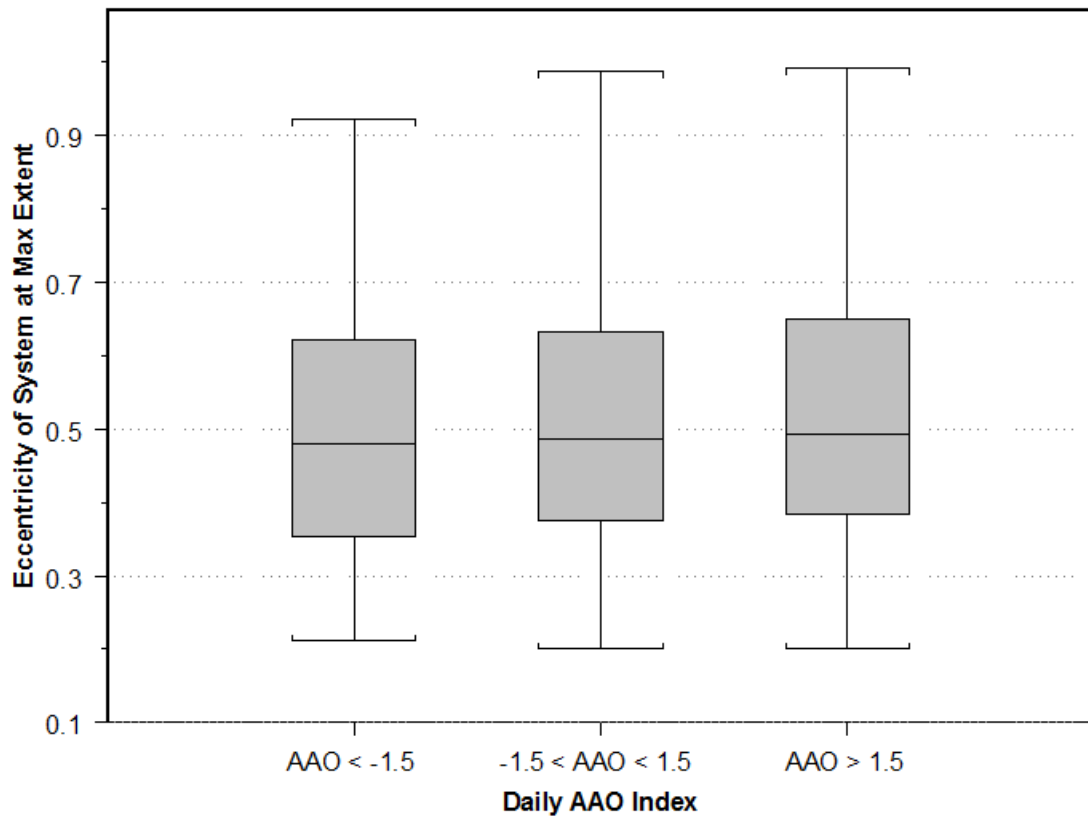


**Fig. 21.** As in figs. 15-17 except for the eccentricity of LLCS cloud shields at their maximum extent.

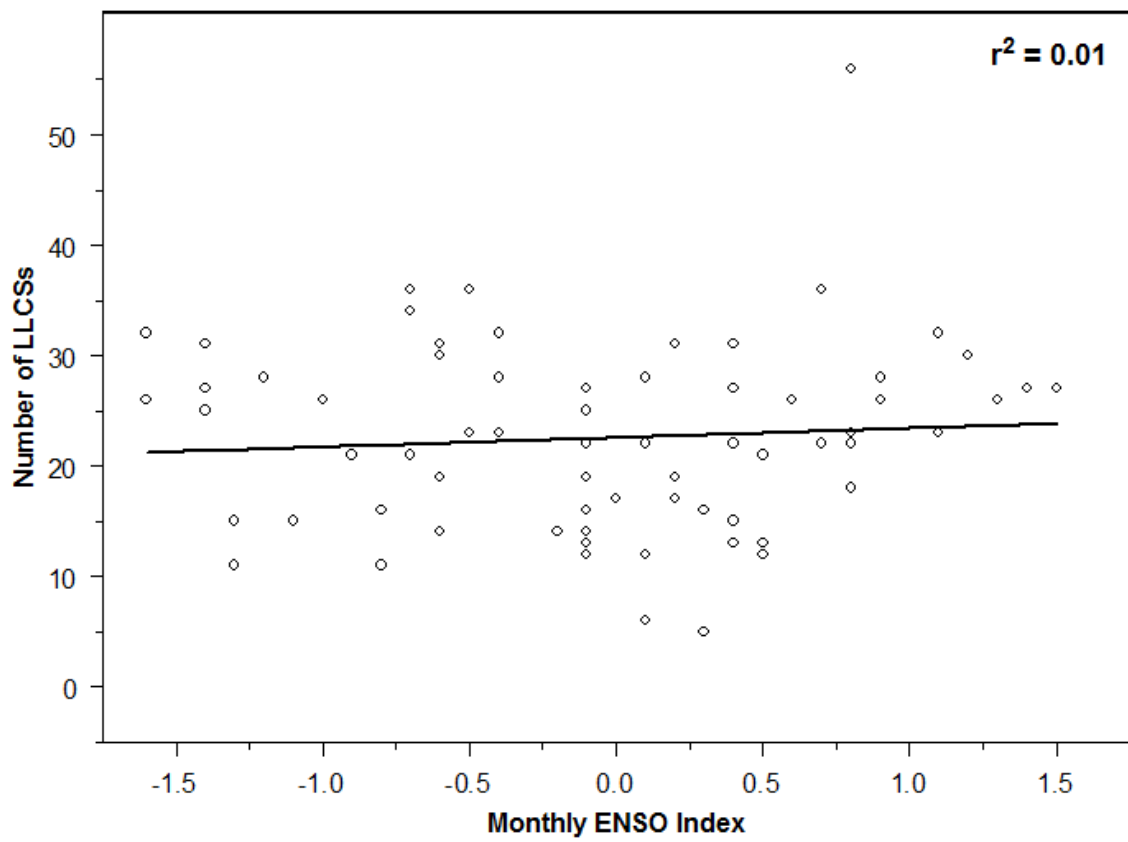


**Fig. 22.** Correlation between number of LLCs during each month and the monthly ENSO index.

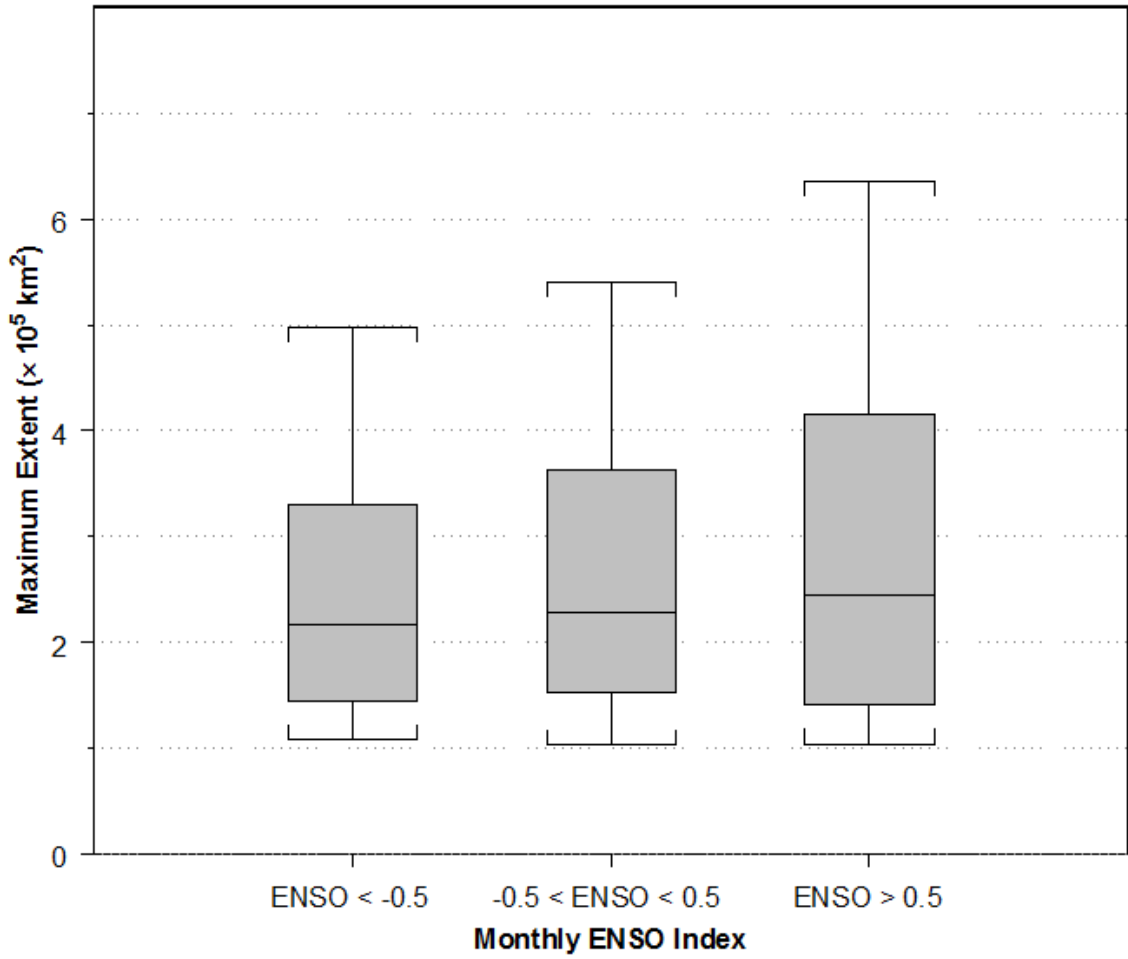


**Fig. 23.** Maximum extent reached by each LLCS during negative, neutral, and positive ENSO phases. Whiskers show the 10<sup>th</sup> and 90<sup>th</sup> percentiles.

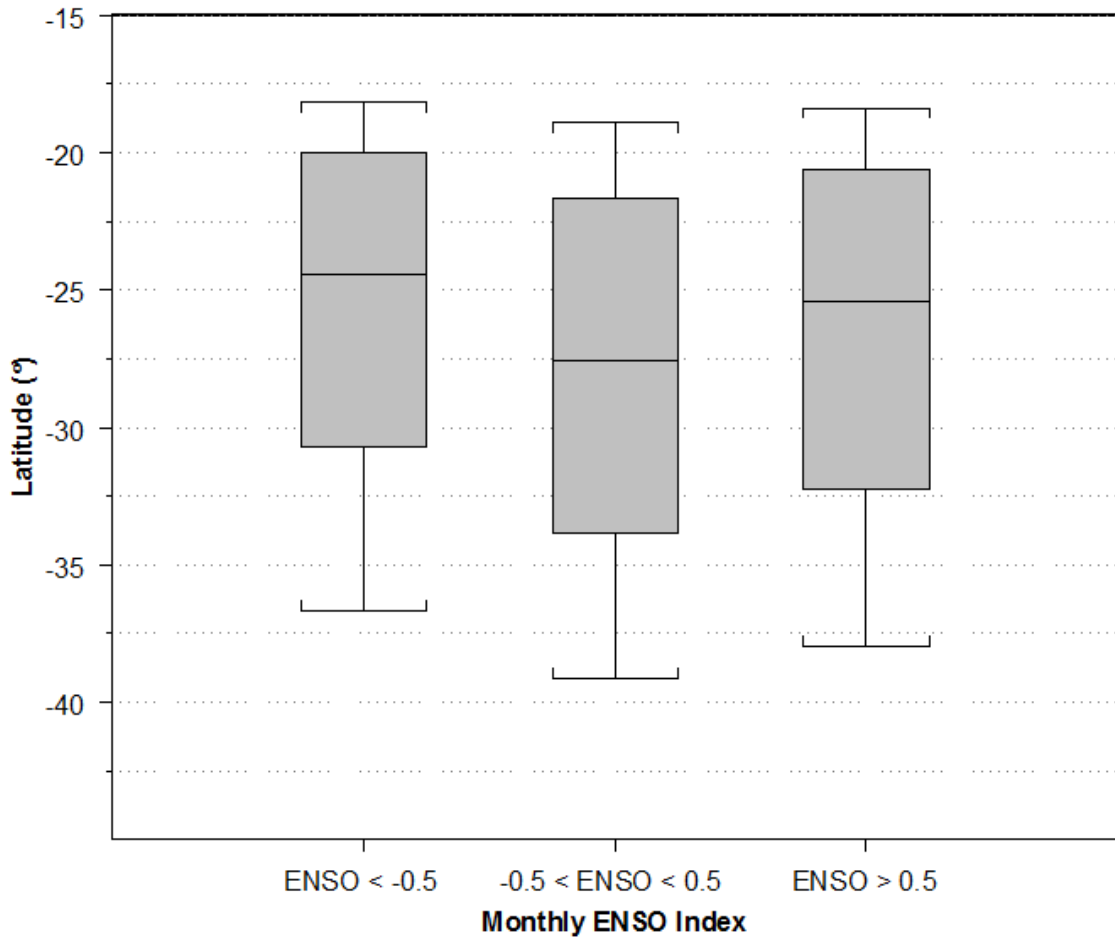


**Fig. 24.** As in fig. 20, except for the latitude of LLCS centroids at maximum extent.

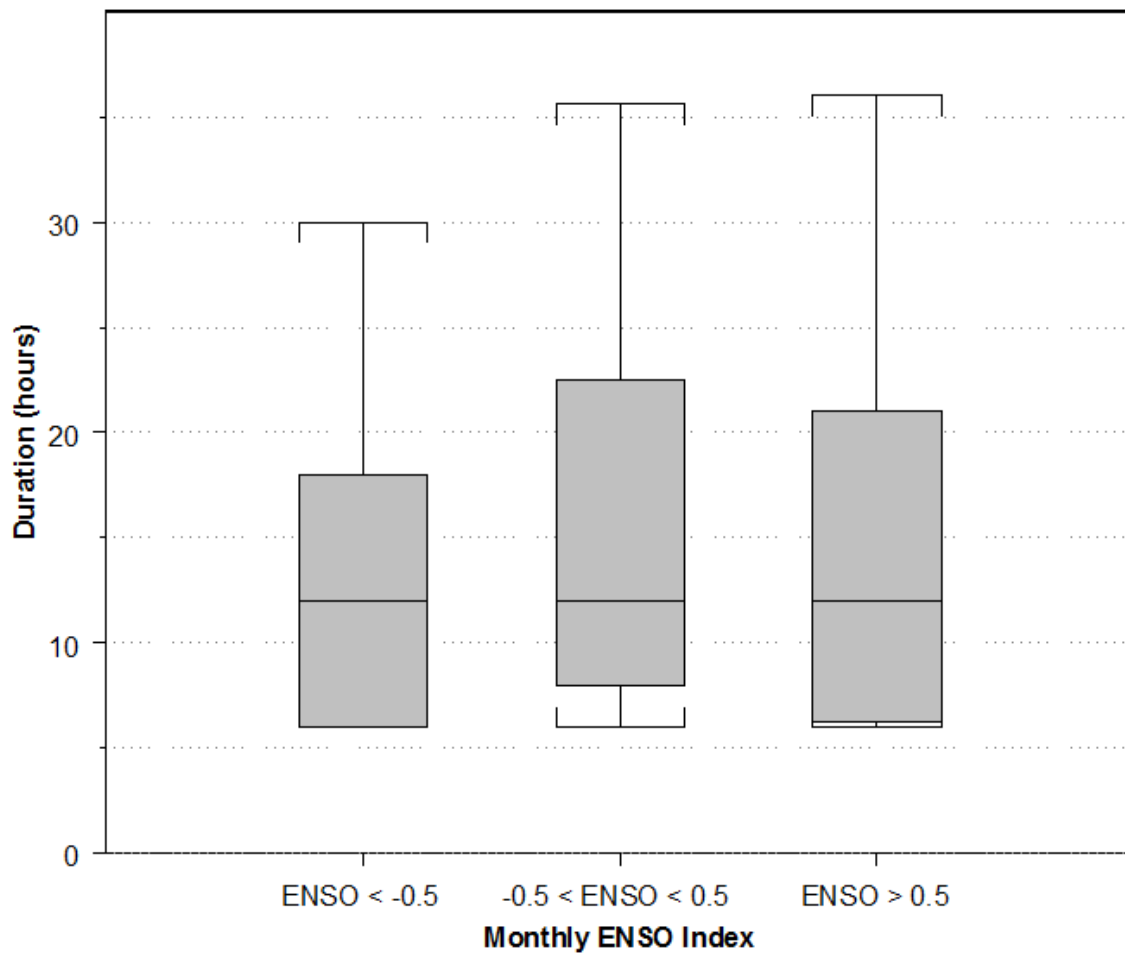


**Fig. 25.** As in figs. 20 and 21, except for LLCS duration.

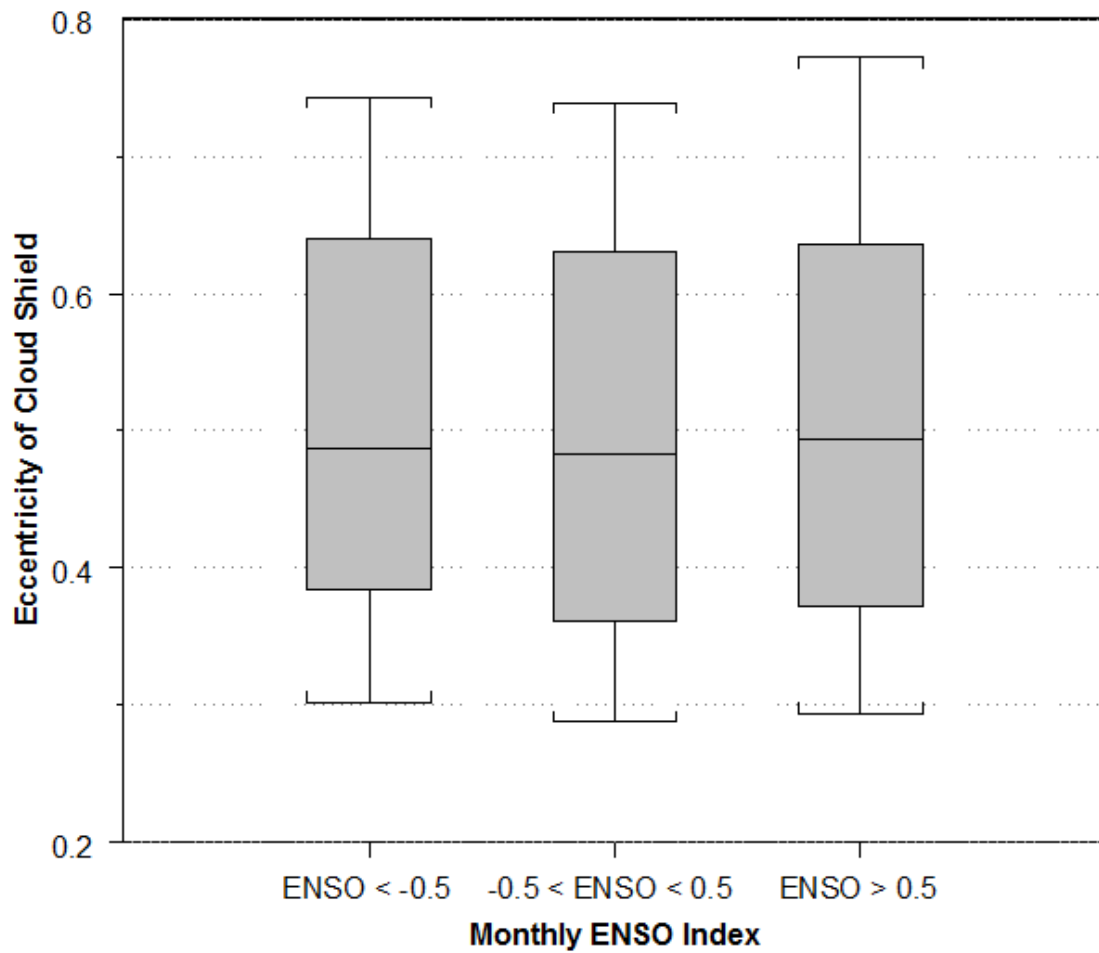


**Fig. 26.** As in figs. 20-22, except for the eccentricity of LLCS cloud shields at maximum extent.



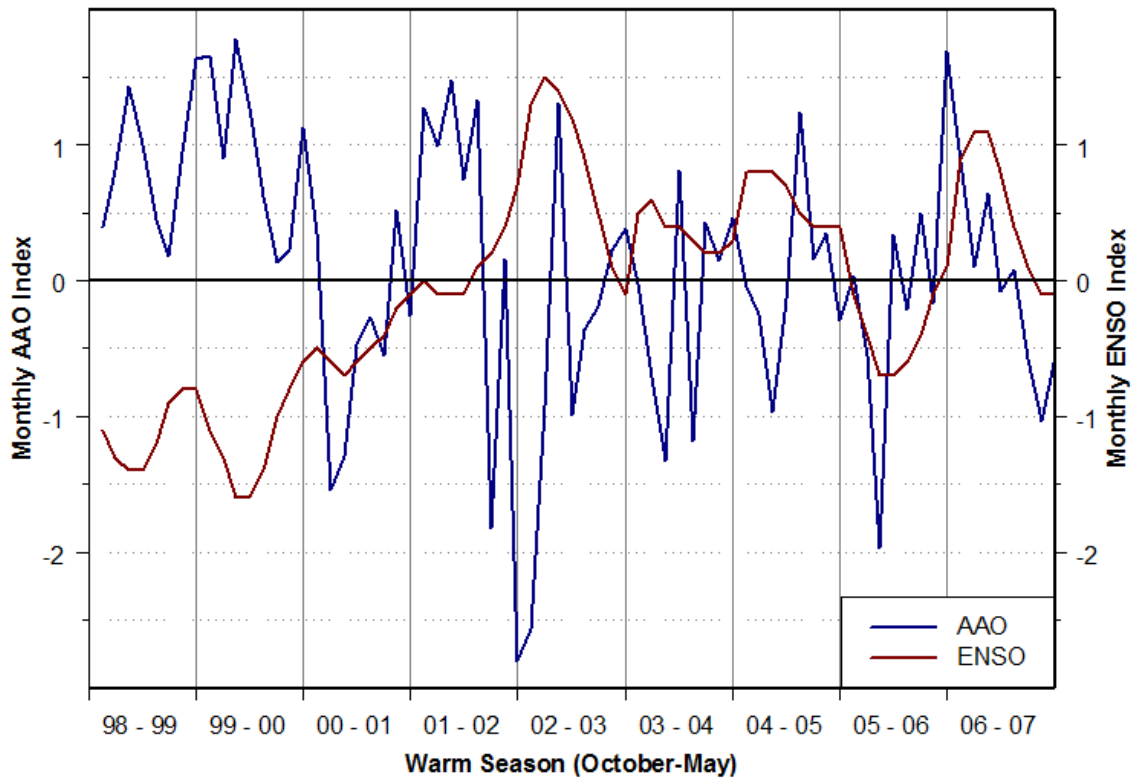


**Fig. 27.** Time series of monthly AAO index and monthly ENSO index for the warm seasons of 1998-2007.

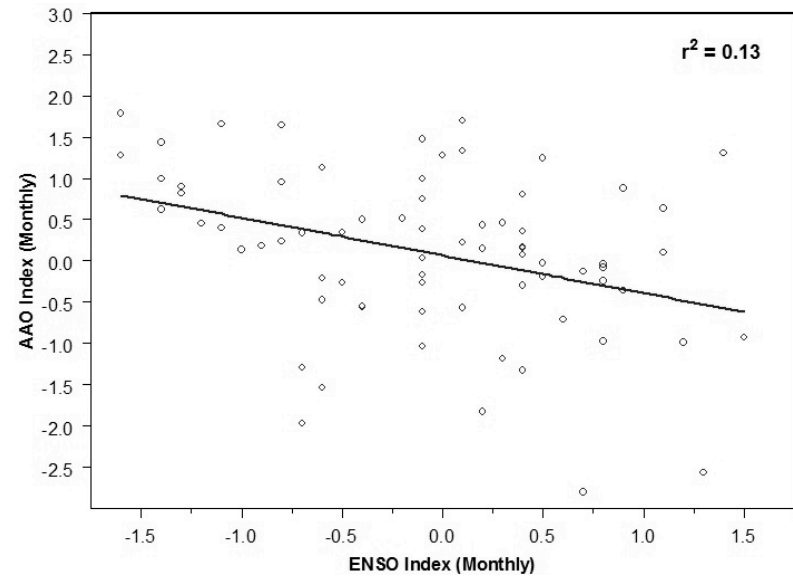
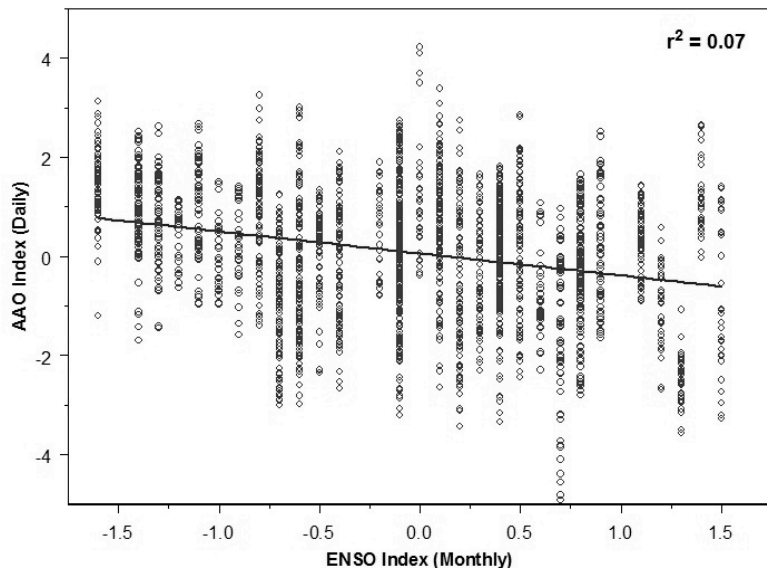


**Fig. 28.** Scatter plots of the relationship between the monthly ENSO index and the daily AAO index (a) and the monthly AAO index (b) for the entire study period.

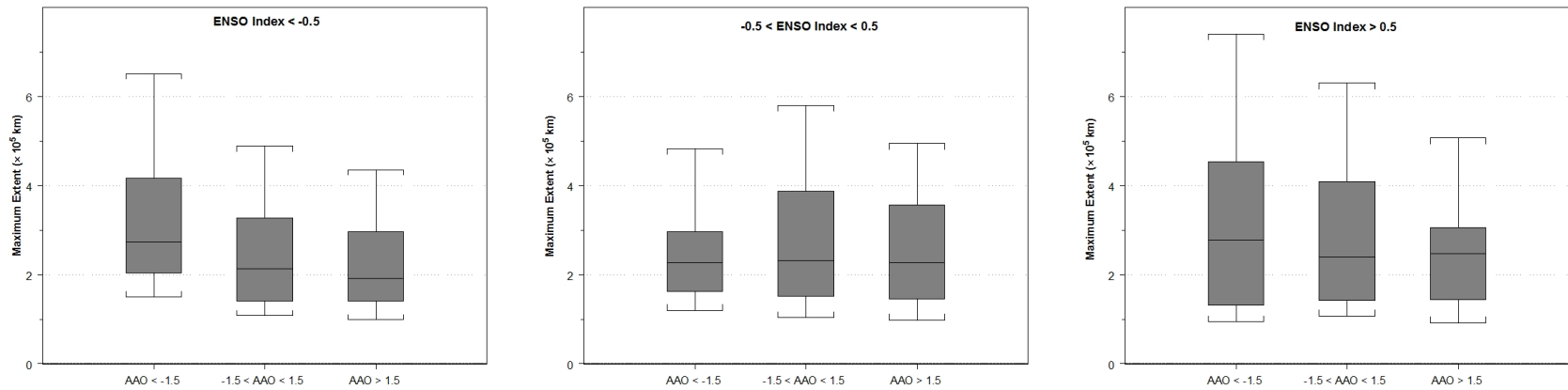


**Fig. 29.** Box plots of the relationship between the daily AAO index and LLCS maximum extent for negative ENSO phases (a), neutral ENSO phases (b), and positive ENSO phases (c). Whiskers show the 10<sup>th</sup> and 90<sup>th</sup> percentiles.

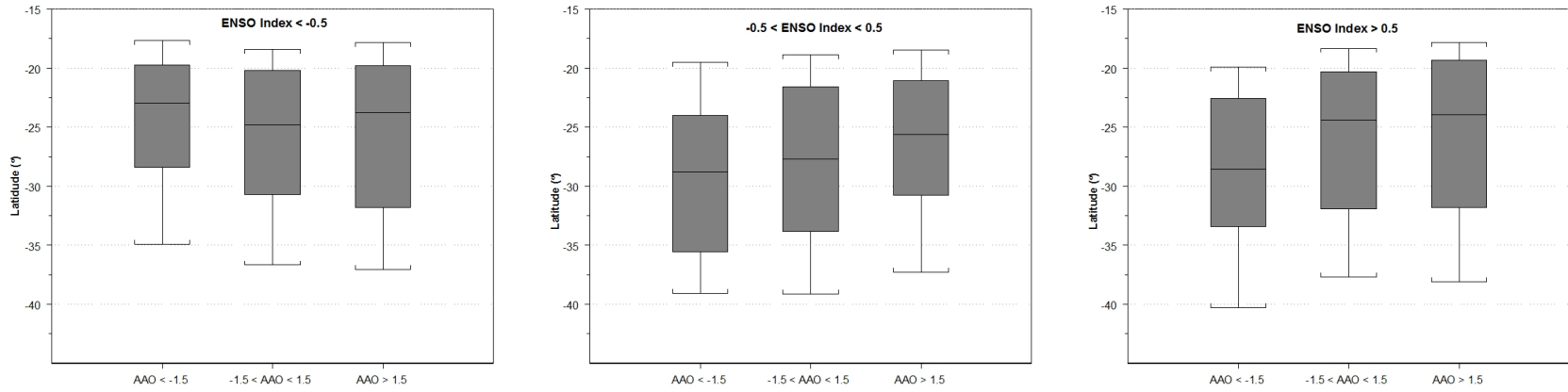


**Fig. 30.** As in fig. 26 except for the latitude of LLCS centroids at maximum extent.

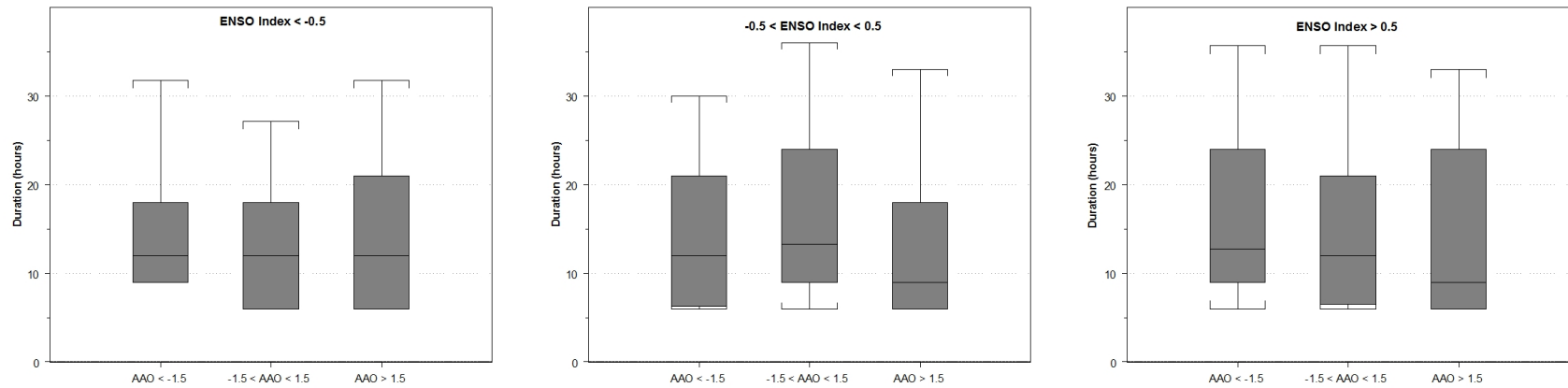


**Fig. 31.** As in figs. 26-27 except for LLCS duration.

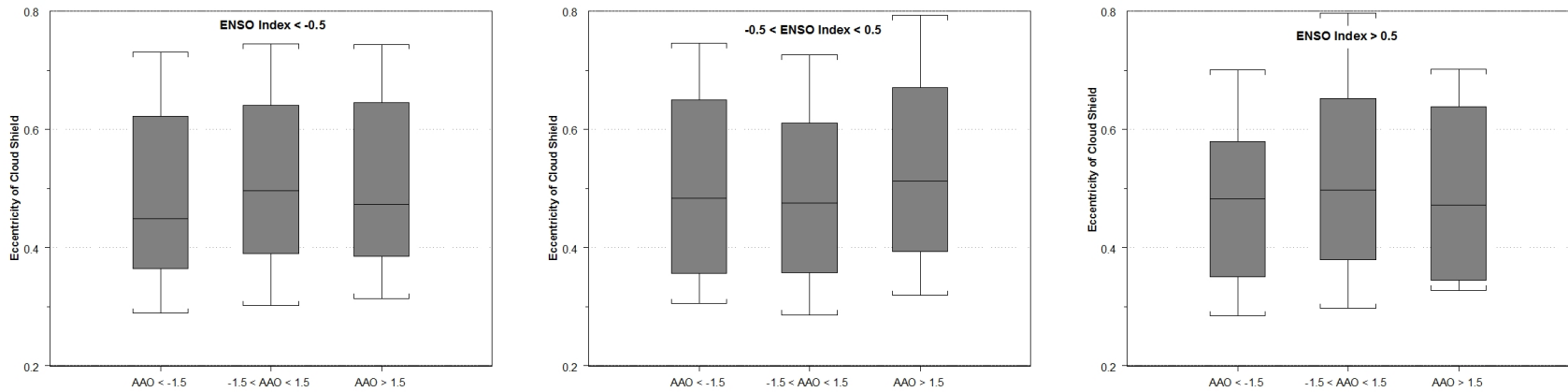


**Fig. 32.** As in figs. 26-28 except for eccentricity of LLCS cloud shields at maximum extent.